MATHEMATICAL SIMULATION OF COLLISION, I

Volume IV of IV

Final Report on Contract FH-11-6685

Appendix C

RFP-142 Project No. 7A

Judith M. Becker

D. Hurley Robbins

HIGHWAY SAFETY RESEARCH INSTITUTE The University of Michigan • Ann Arbor

Prepared under Contract No. FH-11-6685 with the U. S. Department of Transportation, National Traffic Safety Bureau.

Available from the Clearinghouse for Federal Scientific and Technical Information. Inquiries should be directed to the Clearinghouse, Code 410.14, Department of Commerce, Springfield, Virginia 22151, or to any Commerce Field Office.

TABLE OF CONTENTS

Section	Title	Page
A.	Introduction	1
B.	Derivation of Matrix Equation	9
C.	Simulation	17
.1.	Input information	17
.2.	Preliminary calculations	24
.3.	Integration	27
.4.	Generalized forces	30
.a	Centrifugal	33
.b	Gravity	34
.c	Joint	34
.d	Seat	38
.e	Belt	49
.f	Contact	55
.5.	Accelerations	72
.6.	Output calculations	74
.7.	End-of-program test	78
.8.	Input data modification	80
D.	A simple analog to collision between auto occupants	81

LIST OF FIGURES

No.	Title	Page
1	The system - front seat	2
2	Interior layout	5
3	Body angles and pitch	12
4	Body link dimensions	13
5	Body contact dimensions	14
6	Overall flow diagram	18
7	Reference frames	29
8	Generalized force flow diagram	31
9	Cubic joint restraint torque	36
10	Joint injury criterion flow diagram	37
11	Seat geometry	39
12	Seat force flow diagram	40
13	Non-rigid beam seat geometry	42
14	Non-rigid beam seat forces flow diagram	44
15	Rigid beam seat geometry	46
16	Rigid beam seat forces flow diagram	48
17	Lap belt geometry	50
18	Recurrent loading curves	52
19	Belt force flow diagram	53
20	Contact force flow diagram	56
21	Contact geometry	60
22	$T_i(t)$ contact check flow diagram	62
23	Shared deflection contact force flow diagram	64
24	Bi-material contact force flow diagram	66
25	Bi-material loading curve	67
26	Force-injury criteria flow diagram	69
27	Body matrix	73
28	Time end-of-program test	79

LIST OF TABLES

No.	Title	Page
1	Body parameters	19
2	Belt parameters	20
3	Contact surface position parameters	21
4	Material parameters	22
5	Body subscripts	23
6	Joint angle subscript correspondence	35
7	Body segment-contact surface subscript correspondence (i-k)	58
8	i-k correspondence for regular contact	61
9	i-k correspondence for undesired contact	61
10	Contact surface-materials subscript correspondence (k-ℓ)	63
11	i-k correspondence for shared deflection	63

LIST OF PARAMETERS AND BASIC VARIABLES

Symbol	Units	Definition
a	(various)	Body matrix parameters
C'	in.lb	Friction coefficient of body joint
c_s	lb.sec/in	Viscous damping coefficient of seat cushion
D	in.	Length of contact surfaces
D'	in.	Bottoming-out depth of padding
D''	in.	Actual depth of padding
D_{fr}	in.	Distance between front and rear seats
D_i	in.	Inside diameter of steering wheel
D_s	in.	Equivalent length of steering wheel rim in vertical section through driver's arms
E	in-lbs	Absorbed energy of a particular section of the system
E_l	in-lbs	Conserved energy of a particular section of the system
f	lbs	Horizontal friction force on seat cushion
F_c	lbs	Cart stopping force
F_s	lbs	Net vertical seat force on hip
F'_s	lbs	Net vertical force on leg at front edge of seat
F'_{so}	lbs	Static load on front edge of seat cushion
F	lbs	Belt force
FCF	lbs	Injury force causing bone compressive fracture
FSF	lbs	Injury force causing bone shear fracture
FSW	lbs	Force necessary to shatter windshield (Glass Mat'l)
FTD	lbs	Injury force causing tension joint dislocation
g	in/sec^2	Acceleration due to gravity force
G	-	Ratio of residual deformation to maximum deformation
h	in.	Distance from previous body joint to point of action of belt; along center lines of torso for shoulder restraint; as radius of arc of action for lap belt
I	$in\text{-}lb.sec^2$	Moment of inertia of body segment
K	lb/rad	Joint elasticity coefficient
KE_c	in.lb	Kinetic energy of vehicle
KE^c	in.lb	Kinetic energy of segments of body
ℓ	in.	Belt length (projected)
ℓ'	in.	Distance between lap belt anchorage point and hip joint
L	in.	Distance between body segment joints
m_c	$\frac{lb.sec^2}{in}$	Mass of cart
m	$\frac{lb.sec^2}{in}$	Mass of body segment

Symbol	Units	Definition
N	-	Order of polynomial approximation to loading characteristics of materials and belts
NC	-	Maximum number of contact surfaces
NBELT	-	Belt option
NBODY	-	Occupant option
NCART	-	Cart deceleration option
NEND	-	End of program option
NLOAD	-	Loading curve option
NOUT	-	Output variable options
P	lbs	Normal contact force
P'	lbs	Tangential contact force
r	in.	Radius of curvature of body contact arcs
r_A	in.	Ankle radius
R	-	Ratio of energy conserved to that absorbed in belt or contact surface
s	lb/in	Linear spring coefficient at front edge of seat
S	in.	Perpendicular distance from center of body contact arc to contact surface
t	sec	Time
t_m	sec	Time points at which input data are available
t_{max}	sec	Maximum duration of program run
Δt	sec	Length of integration time interval
T	in.	Distance of contact point from contact surface reference point, measured along contact surface
$\hat{T}'$, $\hat{T}$	in.lbs/rad	Linear joint restraint coefficients
v_T	in/sec	Tangential velocity of body contact point along contact surface
W_o	lbs	Static load on seat cushion at hip joint
X	in.	Horizontal joint coordinate (inertial)
x	in.	Horizontal joint coordinate (relative to inside of vehicle)
x"	in.	Horizontal coordinates of contact surface reference points (noninertial)
x_h	in.	Horizontal coordinate of hip relative to space fixed axes, with origin of axes at the initial hip position (inertial)
x_c	in.	Horizontal displacement of center of gravity of vehicle, relative to initial position (inertial)
$\dot{x}_{ho} = \dot{x}_{co}$	in/sec	Initial forward velocity of body and vehicle
Y	in.	Vertical joint coordinate (inertial)
y	in.	Vertical joint coordinate (relative to inside of vehicle)
y"	in.	Vertical coordinates of contact surface reference points (noninertial)

Symbol	Units	Definition
y_h	in.	Vertical coordinate of hip relative to space fixed axes at the initial hip position (inertial)
y_c	in.	Vertical displacement of vehicle center of gravity, relative to initial position (inertial)
z	in.	Horizontal distance from hip joint to front edge of seat cushion (noninertial)
$\hat{z}$	in.	Distance, measured along z from the front of the seat cushion, at which loading changes from linear spring to non-linear spring and damper (noninertial)
α	radians	Angle of body segment centerline relative to true or inertial horizontal
α_o	radians	Angle of shin relative to lower leg center line
β	(various)	Non-linear spring coefficients in seat cushion
γ_o	radians	Angle between top of seat cushion (undeflected) and horizontal reference of vehicle interior
γ_2, γ_3	radians	Angle between line connecting previous joint with center of curvature and torso center line (for back and chest respectively);positive for back, negative for chest
δ	in.	Deformation of belts, contact surface, or body surface
Δ	in.	Slack in belt
ϵ	in.	Residual deformation
η	-	Ratio of D'/D"
θ	radians	Angle of body segment center line to horizontal, relative to inside of vehicle
μ	-	Friction coefficient for seat or contact surface
ξ	$\frac{in}{sec}$; $\frac{rad}{sec}$	Velocity limits for friction in seat, contacts, or joints
ρ	in.	Distance along center line from previous joint to center of gravity of body segment
ρ'	in.	Distance from previous joint to center of curvature of contact arc, along centerline for head
$\sigma_j (j=1-2N)$	(various)	Loading coefficients of belt or contact material
ϕ	radians	Belt angle from horizontal reference, inside vehicle
ϕ'	radians	Angle of ℓ' from horizontal reference, inside vehicle
Φ	radians	Pitch angle of vehicle, positive for front-end down
ψ	radians	Angle of contact surface from horizontal reference, inside vehicle
ω	radians	Minimum angular "limits" in body joint stops, at which joint dislocation would occur
Ω	radians	Maximum angular "limits" in body joint stops, at which joint dislocation would occur

SECTION A. INTRODUCTION

This report is concerned with the mathematical simulation of the motion of an occupant of a motor vehicle which has been involved in an accident. There are three phases to this simulation project. The first phase is quite similar to the Cornell simulation project, differing only in the methods of obtaining certain quantities and in the number of allowed body contacts with the vehicle interior. An Highway Safety Research Institute computer program is currently being used to generate results which are being compared with results from the Cornell program.

The second phase is the main concern of this report. This new model includes all changes and improvements of the earlier model which can be made without increasing the number of degrees of freedom of the system. The vehicle is equipped with a restraint system as shown in Fig. 1. The motion considered occurs only in the forward vertical plane (i.e. in two dimensions) as a result of either forward acceleration (say from a rear-end collision) or deceleration from a front-end collision or sudden stop. A rear-seat passenger and injury potential are considered in this model. It has not yet been programmed for the digital computer but algorithms for doing so are laid out in this report.

The third phase of the simulation project proceeds in two directions. The first is the development of simpler models for the study of specific aspects of the collision problem. The second proceeds in the opposite direction with the objective of further sophisticating the model by the

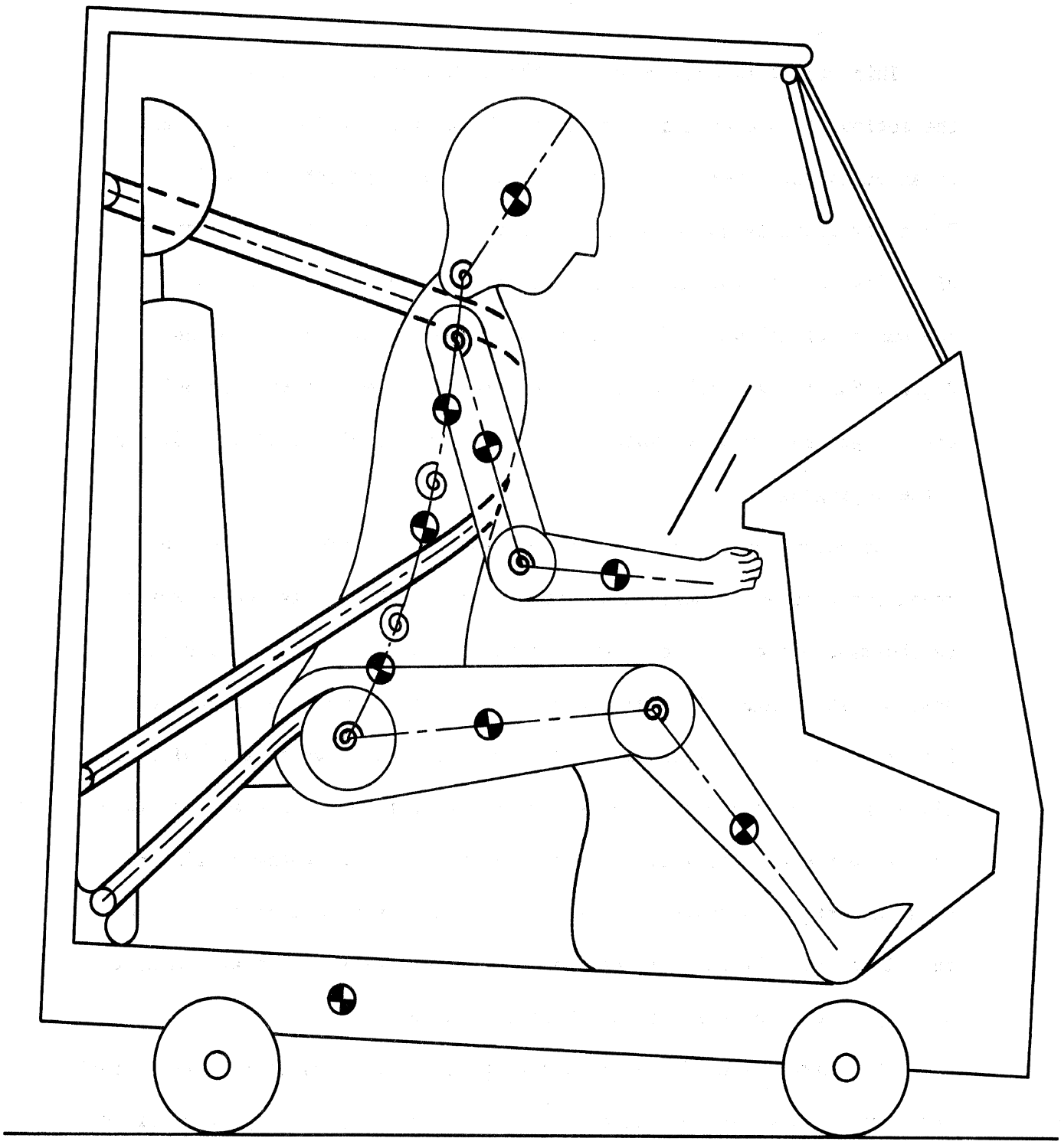

Figure 1

THE SYSTEM - FRONT SEAT

addition of body elasticity, three-dimensional motion, asymetries, and relative vehicle interior motions.

The body of the person is approximated by an eight segment articulated system of links. The eight angles of these segment center lines, which are measured counter-clockwise from the true horizontal, and the two inertial Cartesian coordinates of the hip joint comprise the ten degrees of freedom of the body in the simulations of phases one and two. Phase three will have a larger number of degrees of freedom due to the explicit simulation of such body deformabilities as spine-limb length, shoulder joint motion, and chest-face-abdomen deformations. The phase one program and Cornell ignore these deformabilities while the phase two simulation approximates them by the introduction of injury criteria based on forces. The chest-face-abdomen deformabilities are further approximated by the use of force-deflection loading curves which modify their contact or belt forces. See Section C.4.e and C.4.f for details. These injury criteria can also be used as end-of-program tests, with a program option to specify which of these criteria would be so used. These will be enumerated below. In phases two and three, each of the seven joints of the body is considered to possess torsional elasticity proportional to the relative joint angle, Coulomb friction, and 2-sided angular restraints approximating actual limitations to joint motion. Cornell allows elasticity for only the two spinal joints, with two-sided linear restraints for the neck and spinal joints and one-sided linear restraints for the elbow and knee. The phase one program adds a two-sided linear restraint

for the shoulder and a one-sided one for the hip. The phase two simulation allows the form of the restraints to be linear, cubic, or arbitrary. Again an option in the computer program will specify which of these would be used. See Section C.4.c for details.

The vehicle of phase one and the Cornell vehicle possess one degree of freedom. This is straight-line horizontal motion. Vertical motion and pitch are included in the models of phases two and three. In the former simulation an option exists which specifies whether this horizontal acceleration has an arbitrarily specified time history or whether a cart-stopping-mechanism is used as would be the case with a sled test. The phase two simulation has no such option and all three accelerations must be known time-functions. However, it is possible to include tables for the horizontal, vertical, and angular positions and/or rates as input data and thus eliminate some or all of the vehicle integrations. The phase three simulation will have the option of using explicit differential equations for the three vehicle variables, a three-dimensional cart-stopping-mechanism, or the above tabular data.

The vehicle interior is described by taking several vertical sections through the vehicle, through the center of the occupant, through his legs, and through his arms. These sections are then superimposed to form one composite interior layout, as shown in figure 2. All three phases have an option to specify the position of the person in the vehicle, whether driver, front-seat passenger or rear-seat passenger. Cornell specifies only driver or front-seat passenger by the values of certain contact surface parameters. The Cornell vehicle interior contains only seven contact surfaces, all of which are flat. The phase one program has twelve

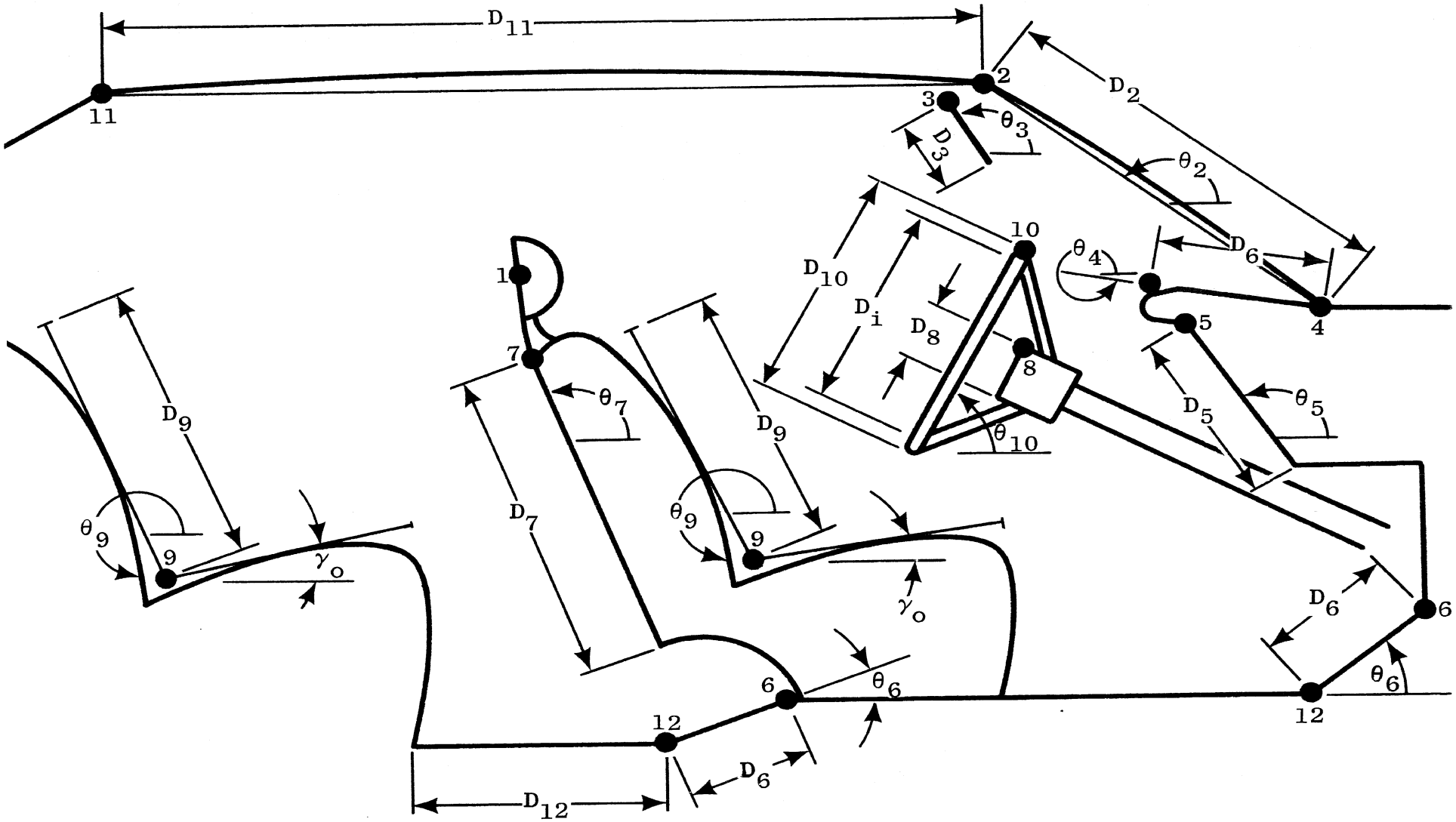

Figure 2

INTERIOR LAYOUT

flat surfaces, while phases two and three have seventeen, some of which may be curved. Cornell considers only seven combinations of contact between particular body segments and contact surfaces. The number of possible contacts in the Highway Safety Research Institute simulations varies with the position of the occupant in the car. In the phase one program the driver has 17 possible contacts, the front-seat passenger 14, and the rear-seat passenger 13. In phases two and three these numbers are 20, 18 and 14 respectively.

The Cornell contact surfaces are assumed to consist of a single material. This is also the case in the phase one program. In phases two and three some of the contact surfaces may be padded, as indicated in Table 10. Cornell and the phase one program have only rigid (non-movable) contact surfaces, while in phase two the motion of the non-rigid ones (for example, the sunvisor, steering wheel rim and column, and head rest) is approximated by force-deflection loading curves and the use of the shared deflection subroutine (Fig. 23). In phase three the non-rigid motion will be expressed in terms of explicit differential equations. All these force-deflection loading curves are assumed to be expressed by fifth-order polynomials in both the deflection and the rate of deflection.

Cornell and the phase one program represent the seat by two systems, one a linear spring whose force acts at the front edge of the seat and the other a linear damper - third order non-linear spring combination whose force acts at the hip joint. Thus this latter force may move along the seat following body motion and might overlap the front edge force. This overlap is prevented in phases two and three either by logic or by using an entirely different seat representation, two possibilities for which are a

rigid beam supported by the present spring-damper systems and a pair of non-rigid beams. In all cases, logic allows the person to fall completely off the seat. Logic in the appropriate sections of the simulations of all three phases automatically differentiates between a person whose feet touch the floor and a child whose legs stick straight out in front of him.

In all cases, the restraint system is composed of a lap belt whose force acts at a constant radial distance from the hip joint and a shoulder restraint whose two forces act at specified points on the body torso center lines. Cornell has an option to specify whether the 3 belt sections and thus the three belt forces are independent, whether the lap belt is independent of the shoulder restraint while the tension forces in the two sections of the shoulder restraint are equal, or whether the forces in all three sections are the same. The phase one program and the phase two simulation assume that the first of these alternatives is true. Phase three will have this option. All three phases have another option to specify how many of the belts are in use, whereas Cornell must use the values of the various belt parameters to do this. The phase one program assumes that the chest wall and abdomen do not deform, while phase two approximates their deformation by load-deflection curves and a shared-deflection subroutine to generate the belt forces. Phase three will have explicit differential equations for their motion.

Cornell and the phase one program do not consider injuries at all. In phase two, the injuries which are considered in the first approximation for non-rigid body segments are joint dislocations, bone fractures, and cuts. Joint dislocations can be of two types; one caused by excessive relative angle and the other by excessive tensile forces across the joint.

Fractures are also of two types; one caused by excessive compressive force along the center line of the bone, the other by excessive shear forces. This last type affects not only the spine and limbs, but also the skull, face, and ribs. Cuts are considered only for head-windshield contact when the glass is actually shattered. These injury criteria will also appear in phase three, though perhaps in different forms.

For all three phases the equations of motion for the system are obtained from the system Lagrangian, which includes the system kinetic energy, potential energy, dissipated energy rate, and the classical generalized non-conservative forces.

SECTION B.

Derivation of Matrix Equation

The body matrix equation, $A\overset{\infty}{\vec{z}} = \vec{b}$, where $\vec{z}$ is the generalized coordinate vector with the ten components α_1 through α_8, x_h and y_h; A is the body matrix as shown in section C.5; and $\vec{b}$ is the generalized force vector whose components are calculated in section C.4, is obtained from the system Lagrangian:

$$\frac{d}{dt}\left[\frac{\partial(KE)}{\partial \dot{z}_i}\right] - \frac{\partial(KE)}{\partial z_i} + \frac{\partial(PE)}{\partial z_i} + \frac{\partial(DE)}{\partial \dot{z}_i} = F_{zi}, \text{ for } i = 1\text{-}10,$$

where KE is the system kinetic energy, PE is its potential energy, DE is its dissipated energy rate, and the F_{zi} are the classical generalized forces, developed in detail in sections C.4.e and C.4.f.

The total body kinetic energy is

$$KE = \frac{1}{2}\sum_{i=1}^{8}\left[m_i(\dot{X}_i^2+\dot{Y}_i^2) + I_i\,\dot{\alpha}_i^2\right]$$

where m_i and I_i are the mass and moment of inertia of the i-th body segment, respectively, α_i is the angle of the i-th body segment center line to the true or inertial horizontal measured counter-clockwise, and X_i, Y_i are the inertial coordinates of the center of gravity of the i-th body segment as follows:

$$X_1 = x_h + \rho_1 \cos\alpha_1 \qquad \dot{X}_1 = \dot{x}_h - \rho_1\dot{\alpha}_1 \sin\alpha_1$$

$$Y_1 = y_h + \rho_1 \sin\alpha_1 \qquad \dot{Y}_1 = \dot{y}_h + \rho_1\dot{\alpha}_1 \cos\alpha_1$$

$$X_2 = x_h + L_1 \cos\alpha_1 + \rho_2 \cos\alpha_2 \qquad \dot{X}_2 = \dot{x}_h - L_1\dot{\alpha}_1 \sin\alpha_1 - \rho_2\dot{\alpha}_2 \sin\alpha_2$$

$$Y_2 = y_h + L_1 \sin\alpha_1 + \rho_2 \sin\alpha_2 \qquad \dot{Y}_2 = \dot{y}_h + L_1\dot{\alpha}_1 \cos\alpha_1 + \rho_2\dot{\alpha}_2 \cos\alpha_2$$

$$X_3 = x_h + L_1 \cos\alpha_1 + L_2 \cos\alpha_2 + \rho_3 \cos\alpha_3$$

$$Y_3 = y_h + L_1 \sin\alpha_1 + L_2 \sin\alpha_2 + \rho_3 \sin\alpha_3$$

$$\dot{X}_3 = \dot{x}_h - L_1\dot{\alpha}_1 \sin\alpha_1 - L_2\dot{\alpha}_2 \sin\alpha_2 - \rho_3\dot{\alpha}_3 \sin\alpha_3$$

$$\dot{Y}_3 = \dot{y}_h + L_1\dot{\alpha}_1 \cos\alpha_1 + L_2\dot{\alpha}_2 \cos\alpha_2 + \rho_3\dot{\alpha}_3 \cos\alpha_3$$

$$X_4 = x_h + L_1 \cos\alpha_1 + L_2 \cos\alpha_2 + L_3 \cos\alpha_3 + \rho_4 \cos\alpha_4$$

$$Y_4 = y_h + L_1 \sin\alpha_1 + L_2 \sin\alpha_2 + L_3 \sin\alpha_3 + \rho_4 \sin\alpha_4$$

$$\dot{X}_4 = \dot{x}_h - L_1\dot{\alpha}_1 \sin\alpha_1 - L_2\dot{\alpha}_2 \sin\alpha_2 - L_3\dot{\alpha}_3 \sin\alpha_3 - \rho_4\dot{\alpha}_4 \sin\alpha_4$$

$$\dot{Y}_4 = \dot{y}_h + L_1\dot{\alpha}_1 \cos\alpha_1 + L_2\dot{\alpha}_2 \cos\alpha_2 + L_3\dot{\alpha}_3 \cos\alpha_3 + \rho_4\dot{\alpha}_4 \cos\alpha_4$$

$$X_5 = x_h + L_1 \cos\alpha_1 + L_2 \cos\alpha_2 + L_4 \cos\alpha_3 + \rho_5 \cos\alpha_5$$

$$Y_5 = y_h + L_1 \sin\alpha_1 + L_2 \sin\alpha_2 + L_4 \sin\alpha_3 + \rho_5 \sin\alpha_5$$

$$\dot{X}_5 = \dot{x}_h - L_1\dot{\alpha}_1 \sin\alpha_1 - L_2\dot{\alpha}_2 \sin\alpha_2 - L_4\dot{\alpha}_3 \sin\alpha_3 - \rho_5\dot{\alpha}_5 \sin\alpha_5$$

$$\dot{Y}_5 = \dot{y}_h + L_1\dot{\alpha}_1 \cos\alpha_1 + L_2\dot{\alpha}_2 \cos\alpha_2 + L_4\dot{\alpha}_3 \cos\alpha_3 + \rho_5\dot{\alpha}_5 \cos\alpha_5$$

$$X_6 = x_h + L_1 \cos\alpha_1 + L_2 \cos\alpha_2 + L_4 \cos\alpha_3 + L_5 \cos\alpha_5 + \rho_6 \cos\alpha_6$$

$$Y_6 = y_h + L_1 \sin\alpha_1 + L_2 \sin\alpha_2 + L_4 \sin\alpha_3 + L_5 \sin\alpha_5 + \rho_6 \sin\alpha_6$$

$$\dot{X}_5 = \dot{x}_h - L_1\dot{\alpha}_1 \sin\alpha_1 - L_2\dot{\alpha}_2 \sin\alpha_2 - L_4\dot{\alpha}_3 \sin\alpha_3 + L_5\dot{\alpha}_5 \sin\alpha_5 - \rho_6\dot{\alpha}_6 \sin\alpha_6$$

$$\dot{Y}_6 = \dot{y}_h + L_1\dot{\alpha}_1 \cos\alpha_1 + L_2\dot{\alpha}_2 \cos\alpha_2 + L_4\dot{\alpha}_3 \cos\alpha_3 + L_5\dot{\alpha}_5 \cos\alpha_5 + \rho_6\dot{\alpha}_6 \cos\alpha_6$$

$$X_7 = x_h + \rho_7 \cos\alpha_7 \qquad \dot{X}_7 = \dot{x}_h - \rho_7\dot{\alpha}_7 \sin\alpha_7$$

$$Y_7 = y_h + \rho_7 \sin\alpha_7 \qquad \dot{Y}_7 = \dot{y}_h + \rho_7\dot{\alpha}_7 \cos\alpha_7$$

$$X_8 = x_h + L_7 \cos\alpha_7 + \rho_8 \cos\alpha_8 \qquad \dot{X}_8 = \dot{x}_h - L_7\dot{\alpha}_7 \sin\alpha_7 - \rho_8\dot{\alpha}_8 \sin\alpha_8$$

$$Y_8 = x_h + L_7 \sin\alpha_7 + \rho_8 \sin\alpha_8 \qquad \dot{Y}_8 = \dot{y}_h + L_7\dot{\alpha}_7 \cos\alpha_7 + \rho_8\dot{\alpha}_8 \cos\alpha_8$$

Figures 3,4 and 5 show the body dimensional parameters and angles; L_i is the link length, ρ_i the distance from the previous joint to the center of gravity, and α_i as above. In figure 3 the axes shown with broken lines are the true, outside, or inertial horizontal and vertical references, while the solid line axes are relative to the interior of the vehicle and are thus inclined at an angle Φ to the inertial axes. This angle Φ is the vehicle pitch angle and is positive for a vehicle having its front end down. The angles of the body segment center lines with the vehicle internal horizontal reference(i.e. the floor) are equal to the inertial angles plus the vehicle pitch angle; i.e. $\Theta_i = \alpha_i + \Phi$. If the vehicle does not pitch, then the reference frames will coincide. In all cases, x_h and y_h are the inertial coordinates of the hip joint.

The potential energy due to joint elasticity, the seat springs (both linear and third-order non-linear) and gravity, respectively, is:

$$PE = \sum_{i=1}^{7} \frac{1}{2}K_i(\alpha_i-\alpha_m+\alpha_{mo}-\alpha_{io})^2 + \frac{1}{2}s(y_1+y_z-y_{zo})^2$$

$$+ \int \sum_{j=1}^{3} \beta_j y_1^j dy_1 + g\sum_{i=1}^{8} m_i(y_i-y_{io}),$$

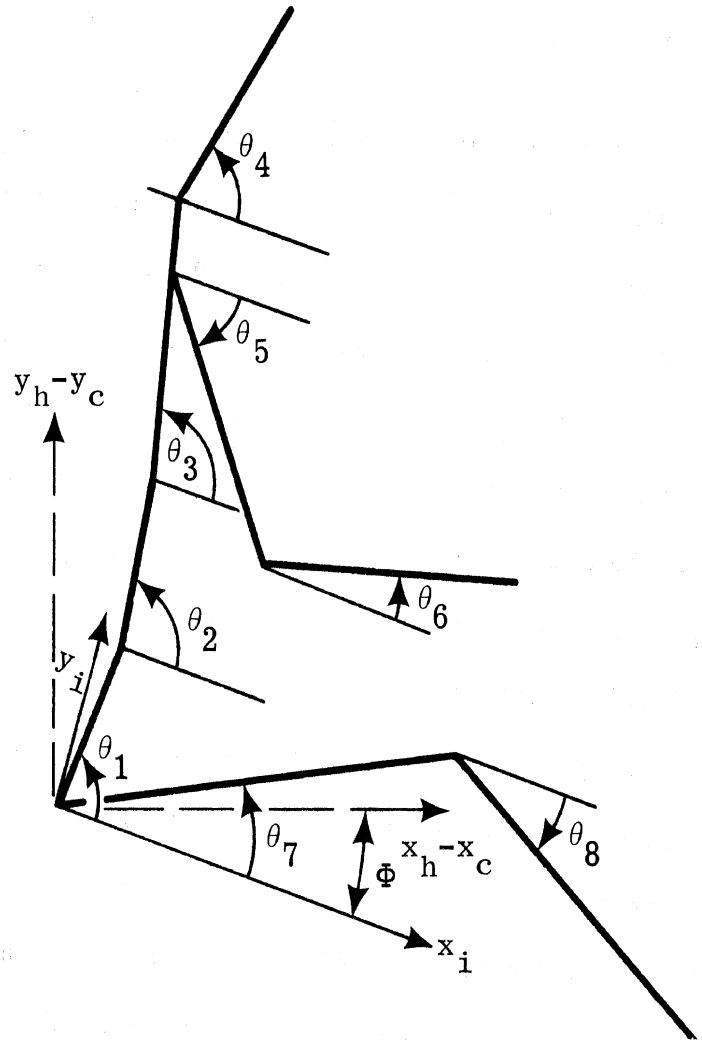

Figure 3

BODY ANGLES AND PITCH

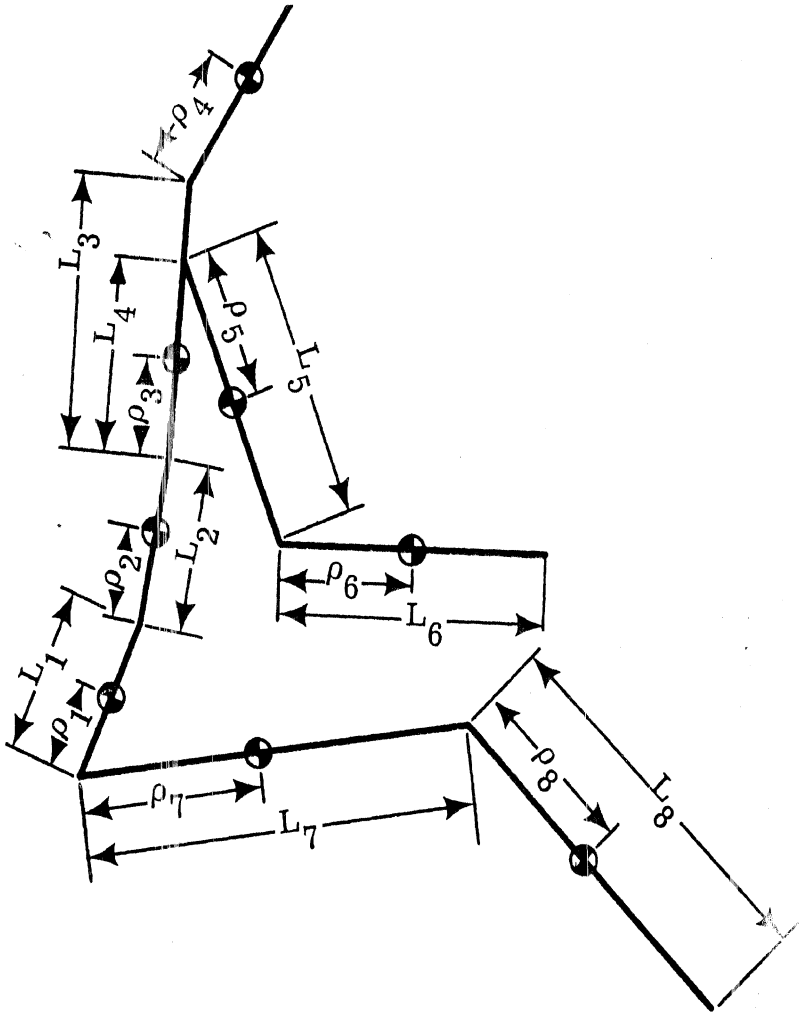

Figure 4

BODY LINK DIMENSIONS

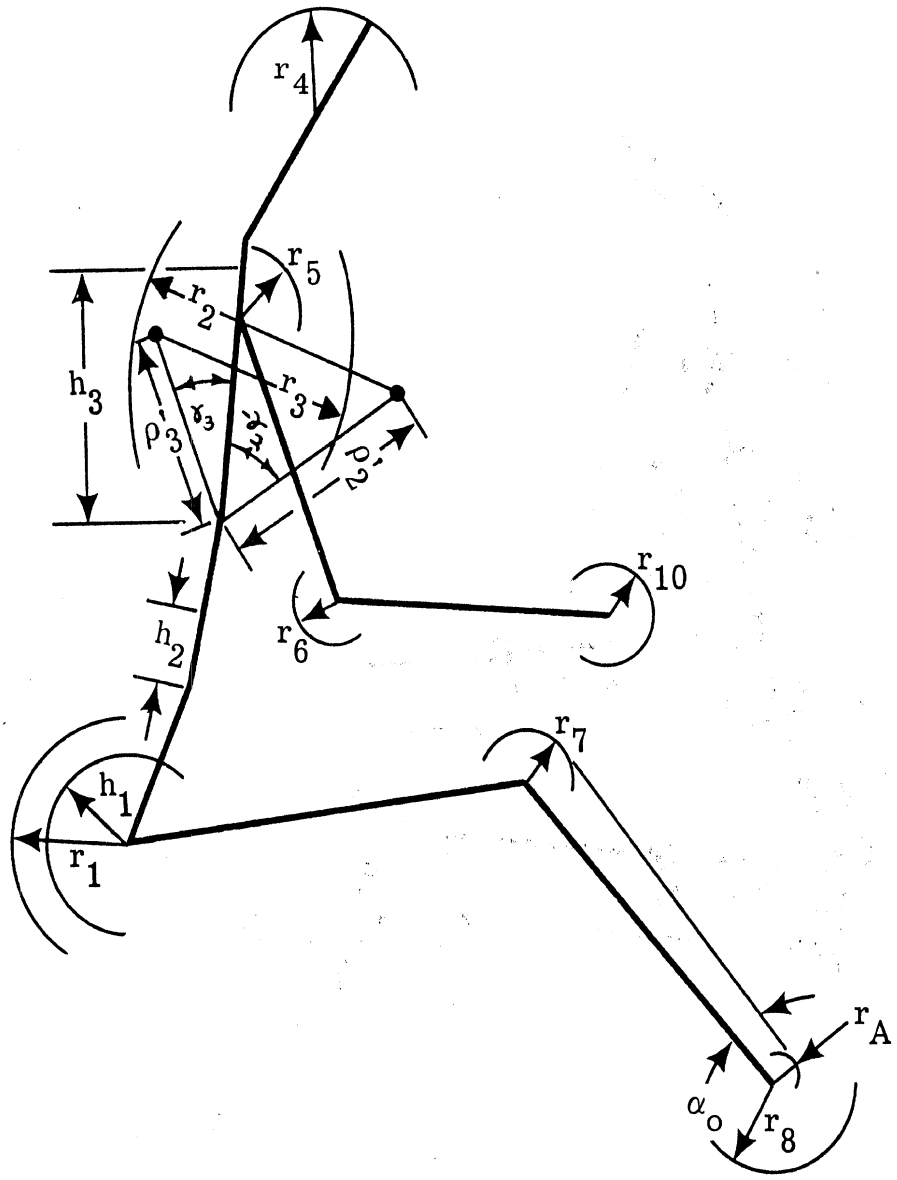

Figure 5

BODY CONTACT DIMENSIONS

where y_1 and y_2 are auxilliary variables to be defined in section C.4.d. In general, potential energy is the integral of the force or torque over the distance (linear or angular) involved. Since these are all well defined functions in the analysis, they can all be directly integrated; even the seat non-linear spring, which gives

$$\sum_{j=1}^{3} \frac{\beta_j y_1^{j+1}}{j+1} .$$

However, if either of the other two seat representations are used, appropriate terms must be substituted.

The dissipated energy rate due to seat friction, the seat damper, joint friction, and the joint restraints, respectively, is:

$$DE = \int_0^{\dot{x}_1} f \, d\dot{x}_1 + \frac{1}{2} c_s \dot{y}_1^2 + \sum_{i=1}^{7} C_i'(\dot{\alpha}_m - \dot{\alpha}_i)\mathrm{sgn}(\dot{\alpha}_m - \dot{\alpha}_i)$$

$$+ \sum_{i=1}^{7} \left[\int_{\dot{\phi}}^{\dot{\phi}+\dot{\alpha}_m} T_i \, d\dot{\alpha}_m - \int_{\dot{\phi}}^{\dot{\phi}+\dot{\alpha}_i} T_i \, d\dot{\alpha}_i \right]$$

In each case here, the rate of energy dissipation is equal to the integral of the force or torque over the velocity (linear or angular). In particular if the joint restraints (section C.4.c. and Fig. 9) do not depend on the angular rates, they could be integrated yielding:

$$\sum_{i=1}^{7} T_i(\dot{\alpha}_m - \dot{\alpha}_i).$$

The F_{zi} are obtained by finding the external forces and moments consisting of the three belt forces, the normal and tangential contact forces, and the pitch. (Sections C.4.e. and C.4.f.).

After differentiation and proper algebraic manipulation, there results a set of ten differential equations in the ten generalized coordinates, which can be recognized as $A \ddot{\vec{z}} = \vec{b}$, where A is a function of $\vec{z}$ and $\vec{b}$ of $\vec{z}$ and $\dot{\vec{z}}$. For ease of calculation $\vec{b}$ is repartitioned into those items calculated in Section C.4.

SECTION C.

SIMULATION

The detailed simulation presented in this section is that of phase two. It incorporates all the additions and changes that can be made to the phase one program without raising the number of degrees of freedom of the system. The overall flow chart for the phase two simulation program is shown in figure 6.

SECTION C.1

INPUT INFORMATION

The general format for the input information is that the various parameters should be grouped according to type. This arrangement allow any one section to be changed by simply substituting new data cards. A complete list of parameters and the basic variables along with their units and definitions will be found just before the introduction, section A.

Arbitrarily specifiable initial conditons are: body position angle (θ_{1o} through θ_{8o}), belt length (ℓ_{jo}) and angle (ϕ_{jo}) for j = 1 through 3, vehicle velocity ($\dot{x}_{co}$).

Vehicle pitch angle, plus its rate and acceleration, and deceleration time-histories are entered in tabular form, as well as vehicle velocity and position, if available. [$\ddot{x}_c(t_m)$, $\ddot{y}_c(t_m)$, $\ddot{\Phi}(t_m)$; with $x_c(t_m)$, $y_c(t_m)$, $\Phi(t_m)$, $\dot{x}_c(t_m)$, $\dot{y}_c(t_m)$, $\dot{\Phi}(t_m)$ if available, for all t_m] The only other vehicle parameters needed at present are its mass (m_c) and moment of inertia (I_c).

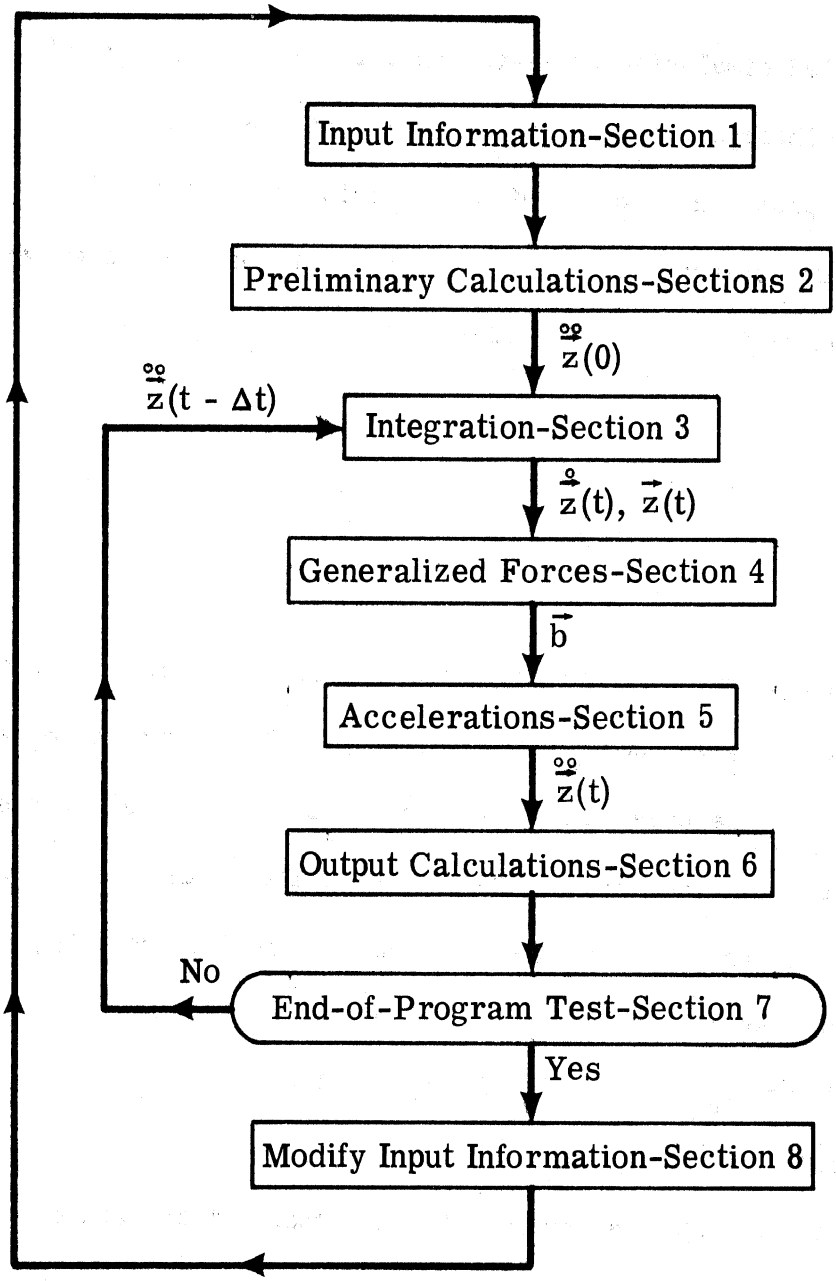

Figure 6

OVERALL FLOW DIAGRAM

subscript	i	1	2	3	4	5	6	7	8	9	10	other
contact radius	r	x	x	x	x	x	x	x	x	x	x	r_A
shear fracture force	FSF	x	x	x	x	x	x	x	x	x		
mass	m	x	x	x	x	x	x	x	x			
inertia	I	x	x	x	x	x	x	x	x			
length	L	x	x	x	x	x	x	x	x			
center of gravity distance	ρ	x	x	x	x	x	x	x	x			
tension dislocation force	FTD	x	x	x	x	x	x	x				
compression fracture force	FCF	x	x	x		x	x	x	x			
coulomb friction coefficient	C'	x	x	x	x	x	x	x				
elasticity	K	x	x	x	x	x	x	x				
friction velocity limit	ξ	x	x	x	x	x	x	x				
minimum joint angle	ω	x	x	x	x	x	x	x				
maximum joint angle	Ω	x	x	x	x	x	x	x				
linear joint stop coefficients	T'	x	x	x	x	x	x	x				
	$\hat{T}'$	x	x	x	x	x	x	x				
center of curvature distance	ρ'		x	x	x							
center of curvature angle from center-line	γ		x	x								

TABLE 1.

Parameters for the body (subscript i), belts (subscript j), contact surface positions (subscript k) and materials (subscript ℓ) are shown in tables 1 through 4, respectively. Table 5 shows the various meanings attached to the body subscript i for the body parameters. The present seat parameters are: c_s, s, β_1, β_2, β_3, z_o, $\hat{z}$, γ_o, W_o, and F'_{so}.

	subscript j		
parameter	1. lap belt	2. lower torso	3. upper torso
h	x	x	x
ℓ_o	x	x	x
ϕ_o	x	x	x
ℓ'_o	x		
ϕ'_o	x		
Δ	x	x	x
N	x	x	x
G	x	x	x
R	x	x	x
σ_n	x	x	x
σ_{n+N}	?	?	?

TABLE 2.

subscript		parameters					
k		x''	y''	Ψ	D	D''	other
1	head rest	x	x	x	x	x	
2	windshield	x	x	x	x	x	
3	sun visor	x	x	x	x	x	
4	upper panel			x	x	x	
5	lower panel	x	x	x	x	x	
6	toeboard	x	x	x	x	x	
7	back of seat	x	x	x	x	x	
8	column	x	x	x	x	x	
9	seat back	x	x	x	x	x	D_{fr}
10	rim	x	x		x	x	D_i, D_s
11	roof					x	
12	floor					x	

TABLE 3.

subscript		parameters							
ℓ		μ	ξ	G	R	N	σ_n	σ_{n+N}	other
1	seat	x	x	x	x	x	x	?	
2	glass	x	x	x	x	x	x	?	FSW
3	padding	x	x	x	x	x	x	?	η
4	floormat	x	x	x	x	x	x	?	η
5	floor	x	x	x	x	x	x	?	
6	metal			x	x	x	x	?	
7	rim	x	x	x	x	x	x	?	
8	headrest	x	x	x	x	x	x	?	
9	visor			x	x	x	x	?	
10	column			x	x	x	x	?	
11	abdomen			x	x	x	x	?	
12	chest			x	x	x	x	?	
13	face			x	x	x	x	?	
14	shoulder			x	x	x	x	?	

TABLE 4.

subscript			bone injury criteria		
i	body segment	joint	contact arc	shear fracture	compression fracture
parameters	m,I,L,ρ	ζ',K,T', $\hat{T}'$,ω,Ω, ξ, FTD	r,ρ',γ	FSF	FCF
1	lower torso	hip	lower back	lower spine	lower spine
2	center torso	lower spine	upper back	center spine	center spine
3	upper torso	upper spine	chest	upper spine	upper spine
4	head	neck	head	skull	
5	upper arm	shoulder	shoulder	back	upper arm
6	lower arm	elbow	elbow	rib	lower arm
7	upper leg	knee	knee	upper leg	upper leg
8	lower leg		foot	lower leg	lower leg
9			shin	face	
10			hand		

TABLE 5.

SECTION C.2

PRELIMINARY CALCULATIONS

In the program for the simulation, certain parameters are computed here and stored for later use, so as to keep the amount of calculation to a minimum. One set comprises the parameters used in calculating the elements of the body matrix (a_i for $i = 1$ to 17); another the initial belt parameters (λ_i for $i = 1$ to 6). Their defining relations are as follows:

$i = 4,6,8 \qquad a_i = m_i \rho_i$

$i = 5,7 \qquad a_i = m_i \rho_i + m_{i+1} L_i$

$i = 1,2 \qquad a_i = m_i \rho_i + L_i \sum_{j=i+1}^{6} m_j$

$a_3 = m_3 \rho_3 + m_4 L_3 + (m_5 + m_6) L_4$

$a_9 = \sum_{j=1}^{8} m_j$

$i = 10,11,12 \qquad a_i = I_{i-9} + m_{i-9} \rho_{i-9}^2 + L_{i-9}^2 \sum_{j=i-8}^{6} m_j$

$a_{12} = I_3 + m_3 \rho_3^2 + m_4 L_3^2 + (m_5 + m_6) L_4^2$

$i = 13,15,17 \qquad a_i = I_{i-9} + m_{i-9} \rho_{i-9}^2$

$i = 14,16 \qquad a_i = I_{i-9} + m_{i-9} \rho_{i-9}^2 + L_{i-9}^2 m_{i-8}$

$$\lambda_1 = \ell'_o \cos\phi'_o \ , \ \lambda_2 = \ell'_o \sin\phi'_o$$

$$\lambda_3 = L_1\sin\theta_{1o} + h_2\sin\theta_{2o} - \ell_{2o}\sin\phi_{2o}$$

$$\lambda_4 = L_1\cos\theta_{1o} + h_2\cos\theta_{2o} - \ell_{2o}\cos\phi_{2o}$$

$$\lambda_5 = L_1\sin\theta_{1o} + L_2\sin\theta_{2o} + h_3\sin\theta_{3o} - \ell_{3o}\sin\phi_{3o}$$

$$\lambda_6 = L_1\cos\theta_{1o} + L_2\cos\theta_{2o} + h_3\cos\theta_{3o} - \ell_{3o}\cos\phi_{3o}$$

Single parameters are the initial lap belt angle and length, and the angle between the shin surface and the lower leg center line. These are defined, respectively, as:

$$\phi_{1o} = \phi_o + \sin^{-1}[h_1/\ell'_o],$$

$$\ell_{1o} = \ell'^2_o - h_1^2 + h_1[\phi'_o - \theta_{1o} + \tfrac{1}{2}\pi],$$

$$\alpha_o = \sin^{-1}[(r_7-r_A)/L_8].$$

Other calculations performed here are of the initial values of the output data variables. Most of these will be zero; eg the head and chest accelerations at their centers of gravity, all energies except kinetic, and all contact forces except those on on the seat back, head rest, floor, and toeboard. Initial kinetic energies are, respectively for the vehicle and body segments:

$$KE_c = \tfrac{1}{2}m_c \dot{x}^2_{co},$$

$$KE_i = \tfrac{1}{2}m_i \dot{x}^2_{co}, \text{ for } i = 1\text{-}8.$$

Initial contact forces are dependent on initial body position (or perhaps vice versa,using the appropriate loading relation for force in terms of deflection with rate of deflection equal to zero).

Lastly the initial accelerations on the body are calculated considering only the initial forces due to gravity, the belts, and the initial contacts. The generalized centrifugal forces, joint torques, and net seat cushion forces are all zero.

The vehicle initial accelerations are read from the tables.

SECTION C.3

INTEGRATION

At present, a four point Adams-Moulton method started with a modified Euler method is used. The Euler method is used to obtain the first three points after the given initial point. Thereafter four points are used in the Adams third difference prediction and correction equations. At each computation of a new point, the iteration continues until successive approximations are within a given tolerance or the iteration has been tried a prescribed number of times.

With an integration option, different schemes could be chosen according to the option. Otherwise the integration would be (and is) carried out by a subroutine.

If, in the input information, tabular data is available only for $\ddot{x}_c(t_m)$, $\ddot{y}_c(t_m)$, and $\ddot{\Phi}(t_m)$, then these must be integrated for the vehicle position and velocity and for its pitch angle and rate. If tabular data is also available for $\dot{x}_c(t_m)$, $\dot{y}_c(t_m)$, $\dot{\Phi}(t_m)$ and/or for $x_c(t_m)$, $y_c(t_m)$, $\Phi(t_m)$, some or all of the integrations for the vehicle may be omitted and the proper values read in from the table.

The body generalized coordinates (x_h, y_h, α_1 - α_8) are now in the inertial reference frame and can be directly integrated twice. The body angles and rates relative to the vehicle interior [$\theta_i(t+\Delta t)$,

$\dot{\theta}_i(t+\Delta t)]$ are obtained by adding $\Phi(t_{m+1})$ and $\dot{\Phi}(t_{m+1})$ to $\alpha(t+\Delta t)$ and $\dot{\alpha}(t+\Delta t)$ respectively.

Figure 7 shows the various reference frames, along with the vehicle center of gravity and body positions at some later time $t=t_m$.

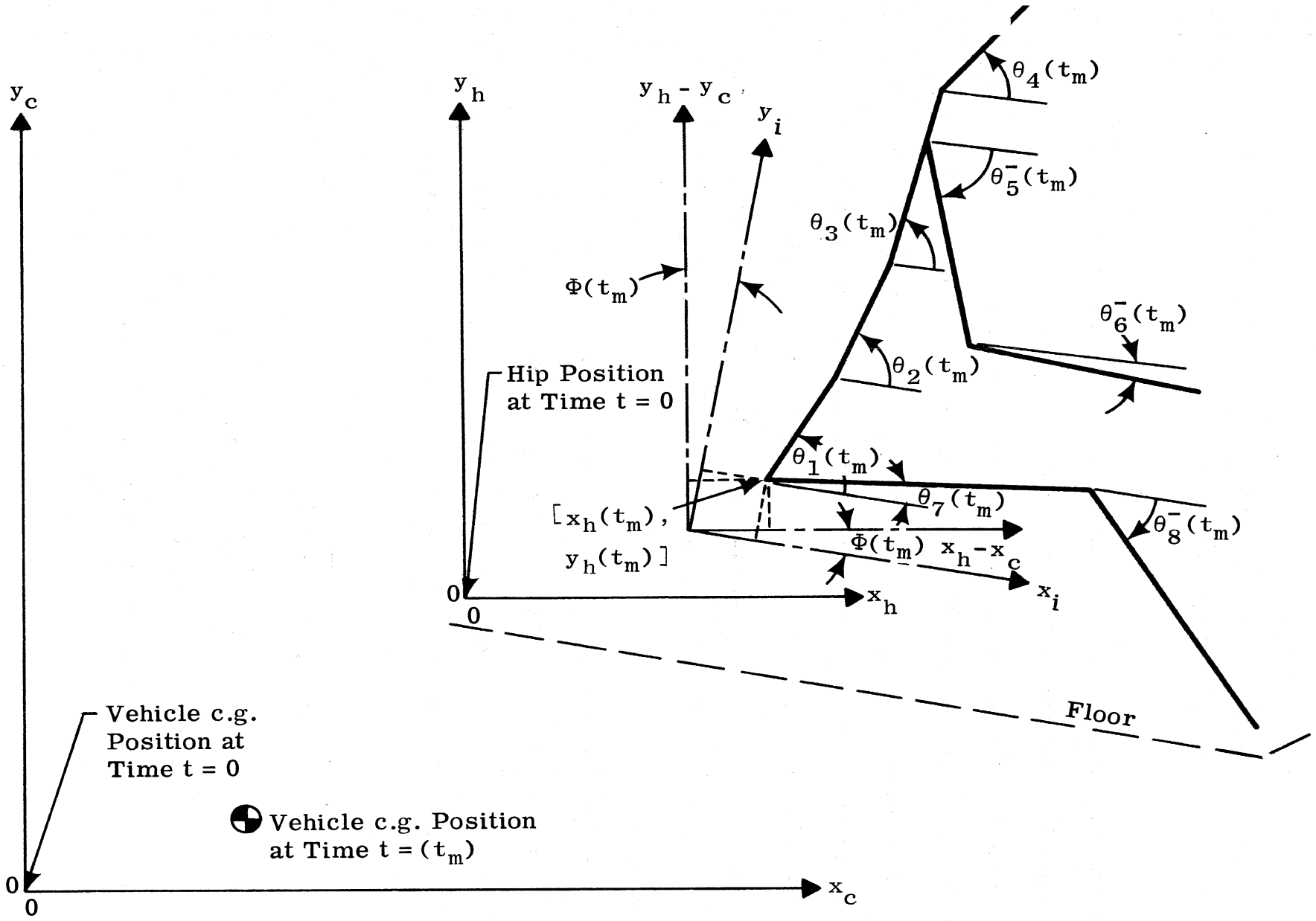

Figure 7

REFERENCE FRAMES

SECTION C.4

GENERALIZED FORCES

Once the set of ten equations in the ten generalized coordinates is obtained for the body motion (see Section B for details), it can be separated so that all the acceleration terms are on one side; i.e. $A\ddot{\vec{z}} = \vec{b}$, where A is a function of $\vec{z}$ and $\vec{b}$ of $\vec{z}$ and $\dot{\vec{z}}$. In order to facilitate the calculation of the components of the vector $\vec{b}$, which is now called the generalized force vector, it is partitioned into sections for the forces and moments due to: 1) centrifugal force, 2) gravity, 3) joint torques, 4) the seat cushion, 5) the belts, and 6) contacts with the interior surfaces of the vehicle, as shown in Fig. 8. In order then,

$$b_i = C_i - G_i + J_i + S_i + B_i + Q_i, \text{ for } i = 1 \text{ to } 10.$$

The vector $\vec{z}$ has as components α_1 through α_8, x_h, and y_h.

In the present case, when the magnitude of the vehicle deceleration is known for each time point, the magnitude of the resulting force on the vehicle is simply:

$$F_c(t_m) = m_c\sqrt{\ddot{x}_c^2(t_m) + \ddot{y}_c^2(t_m)}.$$

The instantaneous positions and velocities of the seven joints, relative to the inside of the vehicle, are needed in several of the subsequent sections. They are calculated from the following relations.

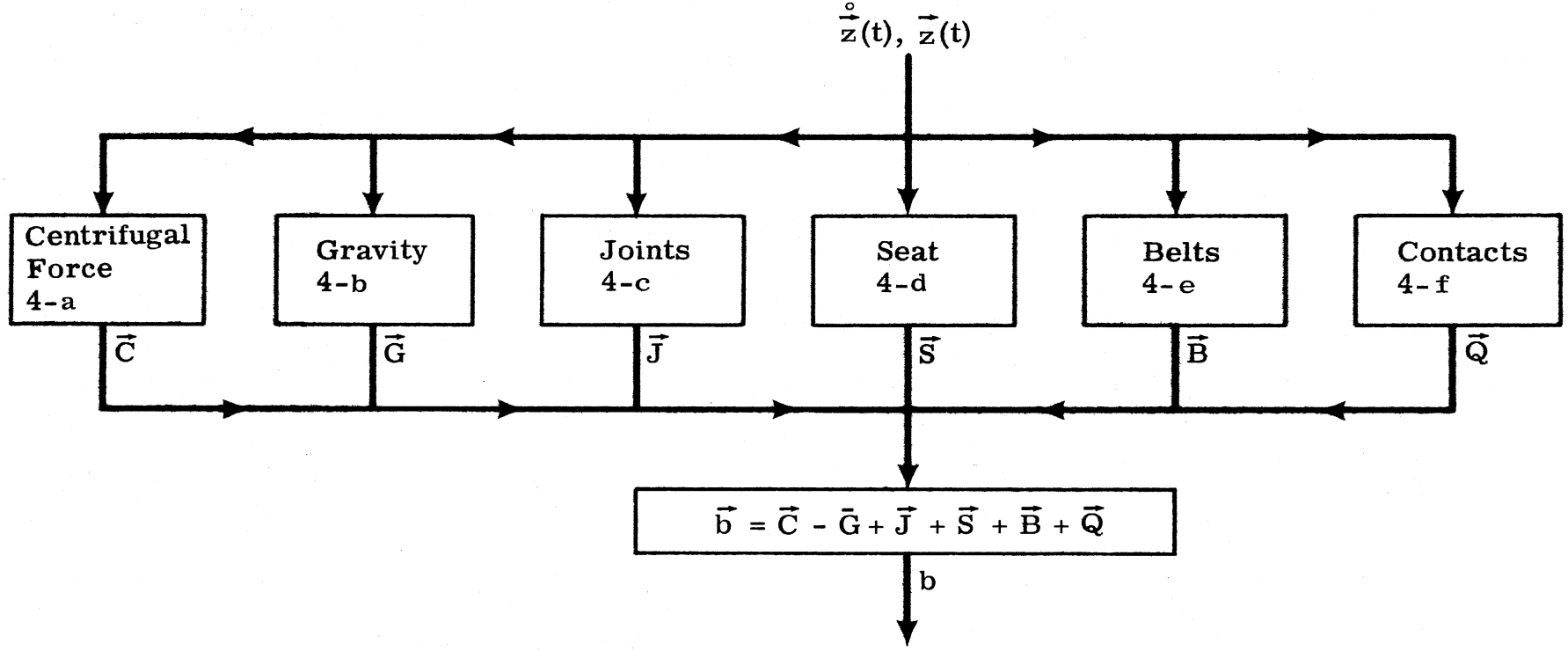

Figure 8

GENERALIZED FORCE FLOW DIAGRAM

hip

i=1 $$x_1(t) = [x_h(t)-x_c(t)]\cos\Phi(t_m)-[y_h(t)-y_c(t)]\sin\Phi(t_m)$$

$$y_1(t) = [x_h(t)-x_c(t)]\sin\Phi(t_m)+[y_h(t)-y_c(t)]\cos\Phi(t_m)$$

and

$$\dot{x}_1(t) = [\dot{x}_h(t)-\dot{x}_c(t)]\cos\Phi(t_m)-[\dot{y}_h(t)-\dot{y}_c(t)]\sin\Phi(t_m)-y_1(t)\dot{\Phi}(t_m)$$

$$\dot{y}_1(t) = [\dot{x}_h(t)-\dot{x}_c(t)]\sin\Phi(t_m)+[\dot{y}_h(t)-\dot{y}_c(t)]\cos\Phi(t_m)+x_1(t)\dot{\Phi}(t_m)$$

knee

i=7 $$x_7(t) = x_1(t)+L_7\cos\theta_7(t)$$

$$y_7(t) = y_1(t)+L_7\sin\theta_7(t)$$

$$\dot{x}_7(t) = \dot{x}_1(t)-L_7\dot{\theta}_7(t)\sin\theta_7(t)$$

$$\dot{y}_7(t) = \dot{y}_1(t)+L_7\dot{\theta}_7(t)\cos\theta_7(t)$$

torso, neck, elbow

i=2,3 $$x_i(t) = x_{i-1}(t) + L_{i-1}\cos\theta_{i-1}(t)$$

4,6 $$y_i(t) = y_{i-1}(t) + L_{i-1}\sin\theta_{i-1}(t)$$

$$\dot{x}_i(t) = \dot{x}_{i-1}(t) - L_{i-1}\dot{\theta}_{i-1}(t)\sin\theta_{i-1}(t)$$

$$\dot{y}_i(t) = \dot{y}_{i-1}(t) + L_{i-1}\dot{\theta}_{i-1}(t)\cos\theta_{i-1}(t)$$

shoulder

i=5 $$x_5(t) = x_3(t) + L_4\cos\theta_3(t)$$

$$y_5(t) = y_3(t) + L_4\sin\theta_3(t)$$

$$\dot{x}_5(t) = \dot{x}_3(t) - L_4\dot{\theta}_3(t)\sin\theta_3(t)$$

$$\dot{y}_5(t) = \dot{y}_3(t) + L_4\dot{\theta}_3(t)\cos\theta_3(t)$$

where $\theta_i(t) = \alpha_i(t) + \Phi(t_m)$.

SECTION C.4.a

CENTRIFUGAL FORCE

In this section are computed those components of $\vec{b}$ which are of the form of angular velocity squared. The specific equations are given below, where:

$$A_{ij}(t) = \dot{\alpha}_j^2(t)\sin[\alpha_j(t) - \alpha_i(t)].$$

$$C_1(t) = L_1 \sum_{j=2}^{6} a_j A_{1j}(t),$$

$$C_2(t) = L_1 a_2 A_{21}(t) + L_2 \sum_{j=3}^{6} a_j A_{2j}(t),$$

$$C_3(t) = a_3 \sum_{j=1}^{2} L_j A_{3j}(t) + L_3 a_4 A_{34}(t) + L_4 \sum_{j=5}^{6} a_j A_{3j}(t),$$

$$C_4(t) = a_4 \sum_{j=1}^{3} L_j A_{4j}(t),$$

$$C_5(t) = a_5 \sum_{j=1}^{2} L_j A_{5j}(t) + a_5 L_4 A_{53}(t) + a_6 L_5 A_{56}(t),$$

$$C_6(t) = a_6 \sum_{j=1}^{2,5} L_j A_{6j}(t) + a_6 L_4 A_{63}(t),$$

$$C_7(t) = a_8 L_7 A_{78}(t),$$

$$C_8(t) = a_8 L_7 A_{87}(t),$$

$$C_9(t) = \sum_{j=1}^{8} a_j \dot{\alpha}_j^2(t)\cos\alpha_j(t),$$

$$C_{10}(t) = \sum_{j=1}^{8} a_j \dot{\alpha}_j^2(t)\sin\alpha_j(t).$$

SECTION C.4.b

GRAVITY

Torque due to gravity in the α_i direction is:

$$G_i(t) = ga_i\cos\alpha_i$$

for i = 1 to 8, where the a_i were defined and calculated in section C.2. In the true horizontal the force is

$$G_g(t) = 0;$$

in the true vertical direction, it is

$$G_{10}(t) = ga_9.$$

SECTION C.4.c

JOINT TORQUES

These torques are caused by joint elasticity, coulomb friction, and angular restraints. The latter two only arise if the relative velocity of the links about a joint exceeds some limit ξ, usually about .01 radians per second. There are no forces due to joint torques in the horizontal and vertical direction. The equations for the generalized forces in the α_i directions are as follows.

i=9,10 $\quad J_i(t) = 0,$

i=8 $\quad J_8(t) = K_7[\alpha_7(t) - \alpha_8(t) + \alpha_8(0) - \alpha_7(0)] - \hat{J}_7(t),$

i=4,6 $\quad J_i(t) = K_i[\alpha_{i-1}(t) - \alpha_i(t) + \alpha_i(0) - \alpha_{i-1}(0)] + \hat{J}_i(t),$

$$i=1,2,5 \quad J_i(t) = (K_i + K_{i+1})[\alpha_i(0) - \alpha_i(t)] + K_{i+1}[\alpha_{i+1}(t)-\alpha_{i+1}(0)] + K_i[\alpha_m(t)-\alpha_m(0)] + \hat{J}_i(t) - \hat{J}_{i+1}(t),$$

$$i=7 \quad J_7(t) = K_7[\alpha_8(t) - \alpha_7(t) + \alpha_7(0) - \alpha_8(0)] - K_1[\alpha_7(t) - \alpha_1(t) + \alpha_1(0) - \alpha_7(0)] + \hat{J}_7(t) - \hat{J}_1(t),$$

$$i=3 \quad J_3(t) = (K_3 + K_4 + K_5)[\alpha_3(0) - \alpha_3(t)] + K_3[\alpha_2(t) - \alpha_2(0)] + K_4[\alpha_4(t) - \alpha_4(0)] + K_5[\alpha_5(t) - \alpha_5(0)] + \hat{J}_3(t) - \hat{J}_4(t) - J_5(t),$$

where for i = 1-7:

$$\hat{J}_i(t) = 0 \text{ for } |\dot{\alpha}_i(t) - \dot{\alpha}_m(t)| < \xi_i,$$

$$\hat{J}_i(t) = C_1' \operatorname{sgn}[\dot{\alpha}_m(t)-\dot{\alpha}_i(t)] + T_i(t) \text{ otherwise.}$$

The specific form of the angular restraint torques may vary, but its general form is shown in Fig. 9. The simplest and most usually used form is linear. An actual restraint curve for the upward motion of the lower leg about the knee joint, as found by J. W. Smith (ref. 4), is also shown in Fig. 9. A cubic fits this curve quite well. Table 6 shows the joint angle subscript correspondence.

i	1	5	7	2,3,4,6
m	7	3	8	i-1

TABLE 6

One of the injury criteria used as an end-of-program test can be applied here. This is joint dislocation due to excessive relative angle. Its flow diagram is shown in Fig. 10.

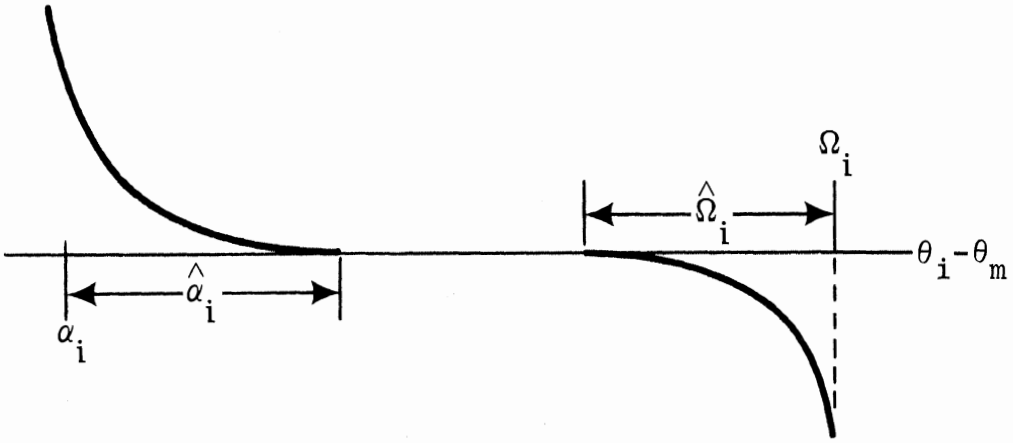

$$T_i = \hat{T}_i \left[\alpha_i + \hat{\alpha}_i) - (\theta_i - \theta_m)\right]^3 \text{ for } \theta_i - \theta_m < \alpha_i + \hat{\alpha}_i$$
$$\text{and } \dot{\theta}_i < \dot{\theta}_m - \xi_i$$

$$T_i = \hat{T}_i' \left[(\theta_i - \theta_m) - (\Omega_i - \hat{\Omega}_i)\right]^3 \text{ for } \theta_i - \theta_m > \Omega_i - \hat{\Omega}_i$$
$$\text{and } \dot{\theta}_i > \dot{\theta}_m + \xi_i$$

$T_i = 0$ Otherwise

for i = 7, $\hat{T}_i$ =-474.7 ''#/rad, α_7 = -0.21 rad, $\hat{\alpha}_7$ = 0.56 rad

Figure 9

CUBIC JOINT RESTRAINT TORQUE

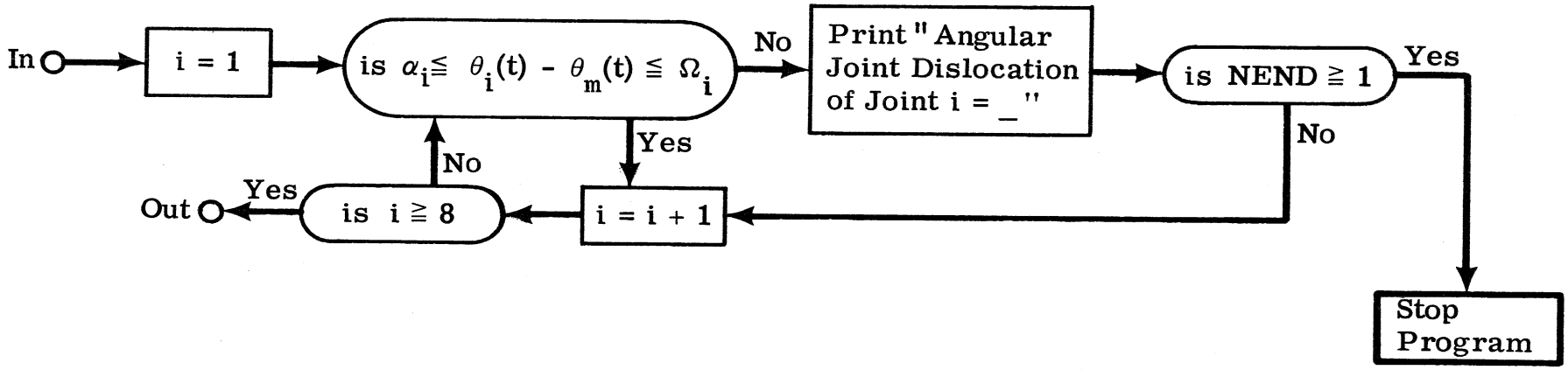

Figure 10

JOINT INJURY CRITERION FLOW DIAGRAM

SECTION C.4.d

SEAT FORCES

The present representation of the seat is that it is composed of a linear spring whose force acts vertically on the upper or lower leg at the front edge of the seat, plus a nonlinear spring and linear damper whose combined force acts vertically on the hip joint. This is the interior vertical, not the true direction. There is also friction proportional to their sun which acts horizontally (also noninertially) at the hip joint. Logic in the simulation allows for falling off the seat, differentiates between adults and children, and prevents the overlapping of the two types of forces. This last is accomplished by assuming that, at some distance $\hat{z}$ from the front edge of the seat, its representation changes from this combination to a linear spring whose spring constant is dependent on the conditions at the previous time instant.

Figure 11 depicts these various cases; figure 12 shows the flow diagram by which the net forces on the body are calculated for each case. The parameter y_{zo} has already been defined and calculated in Section C.2. The generalized force equations in terms of these net seat forces plus the friction are as follows:

$$S_i(t) = 0 \text{ for } i = 1\text{-}6,$$

$$S_7(t) = F_s'(t)\frac{\partial y_z}{\partial \alpha_7}, \quad S_8(t) = F_s'(t)\frac{\partial y_z}{\partial \alpha_8},$$

$$S_9(t) = F_s'(t)\frac{\partial y_z}{\partial x_h} + [F_s'(t)+F_s(t)]\sin\Phi(t_m) - f(t)\cos\Phi(t_m),$$

(A) For $z(t) > \hat{Z}$

For $z(t) \leqq L_7 \cos \theta_7(t)$

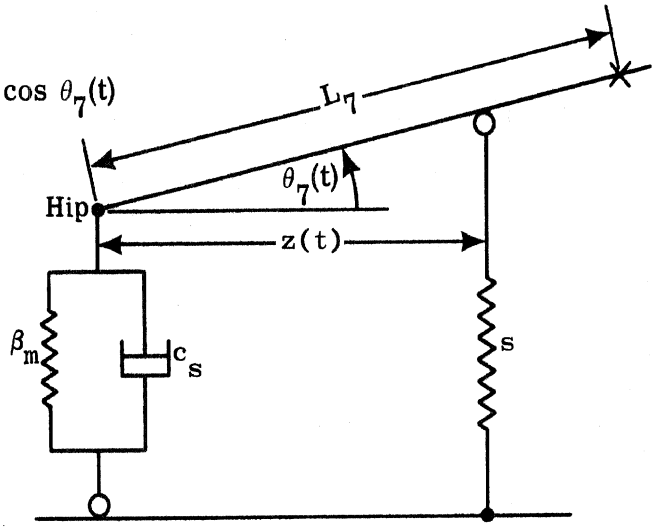

For $z(t) > L_7 \cos \theta_7(t)$

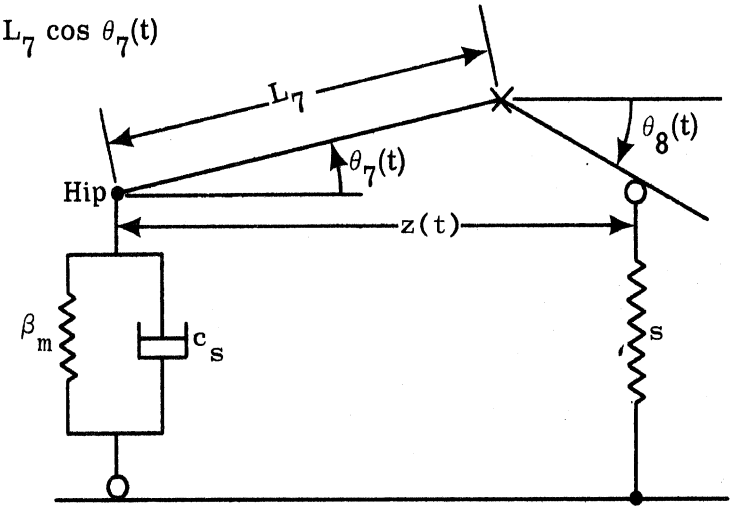

(B) For $0 \leqq z(t) \leqq \hat{z}$

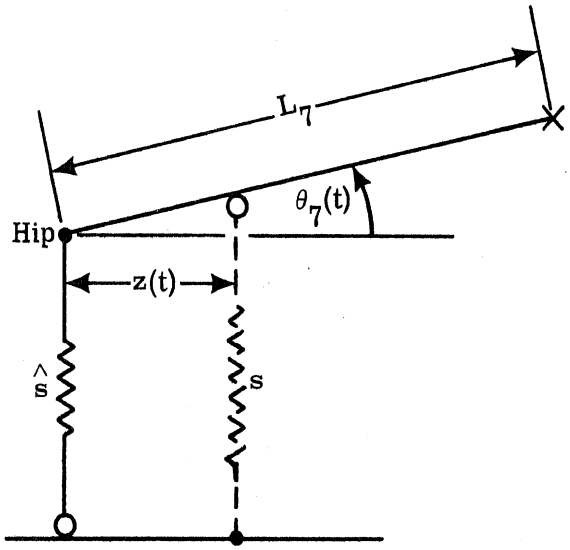

Figure 11

SEAT GEOMETRY

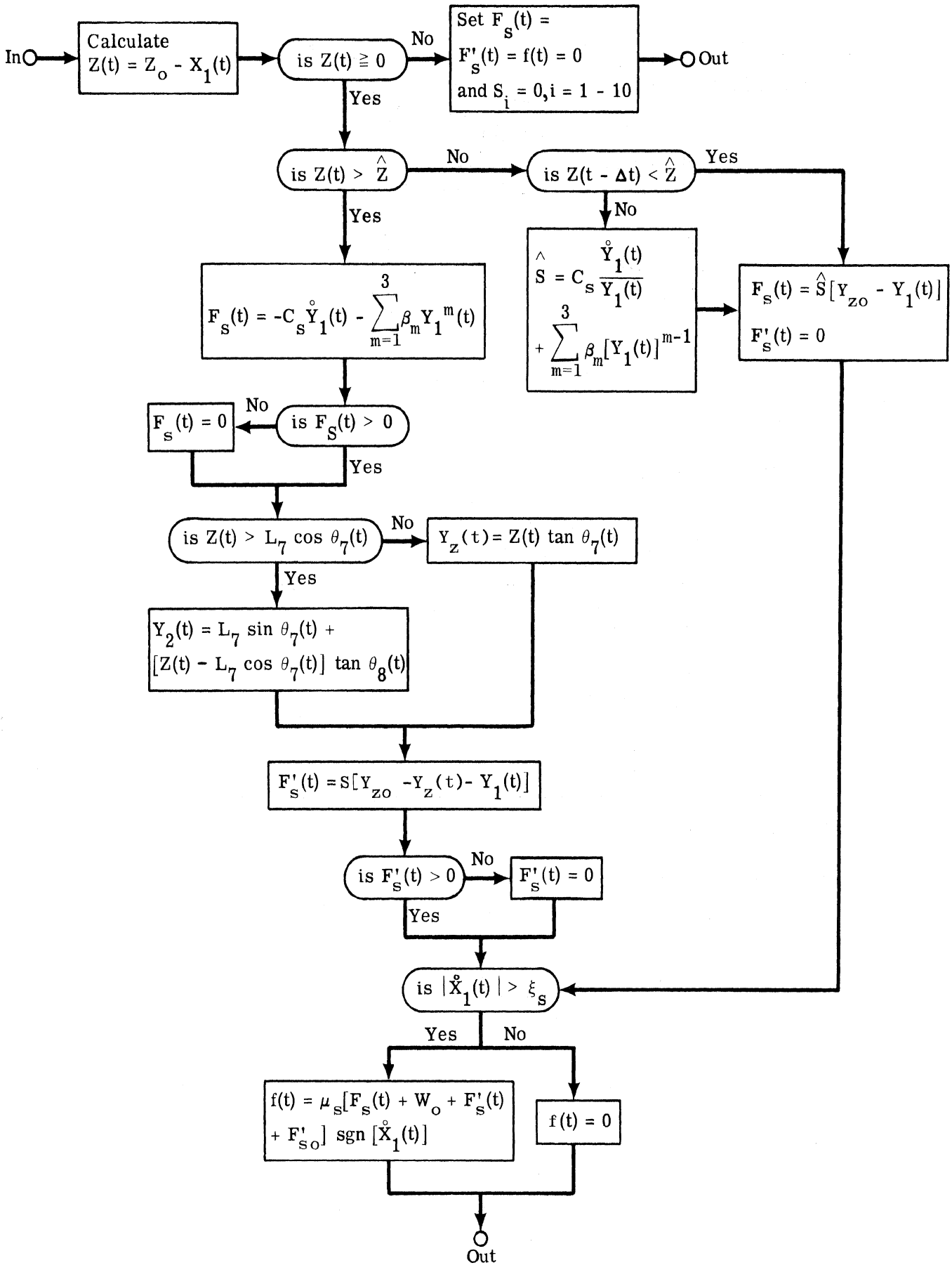

Figure 12

SEAT FORCE FLOW DIAGRAM

$$S_{10}(t) = F_s'(t)\frac{\partial y_z}{\partial y_h} + [F_s'(t)+F_s(t)]\cos\Phi(t_m) + f(t)\sin\Phi(t_m),$$

where, for $z(t) \leq L_7\cos\theta_7(t)$,

$$\frac{\partial y_z}{\partial \alpha_7} = z(t)\sec^2\theta_7(t), \quad \frac{\partial y_z}{\partial \alpha_8} = 0$$

$$\frac{\partial y_z}{\partial x_h} = -\cos\Phi(t_m)\tan\theta_7(t), \quad \frac{\partial y_z}{\partial y_h} = \sin\Phi(t_m)\tan\theta_7(t)$$

and for $z(t)$ $L_7\cos$ $_7(t)$,

$$\frac{\partial y_z}{\partial \alpha_7} = L_7[\cos\theta_7(t)+\sin\theta_7(t)\tan\theta_8(t)],$$

$$\frac{\partial y_z}{\partial \alpha_8} = [z(t)-L_7\cos\theta_7(t)]\sec^2\theta_8(t),$$

$$\frac{\partial y_z}{\partial x_h} = -\cos\Phi(t_m)\tan\theta_8(t), \quad \frac{\partial y_z}{\partial y_h} = \sin\Phi(t_m)\tan\theta_8(t),$$

where $\theta_i(t) = \alpha_i(t) + \Phi(t_m)$.

Another method of preventing overlap is to change the representation of the seat to be either that of a non-rigid beam or that of a rigid beam supported at fixed points by the present spring and spring-damper systems. In both cases the equations of motion will be different.

Another possible representation for the seat cushion is that of a non-rigid beam. In particular it will be assumed to consist of a pair of uniform beams; one of length ℓ and supported at both ends and the other of length $k\ell$ cantilevered at a fixed distance equal to its length from the front edge of the other beam and thus of the seat. The two beams and the resulting system are depicted in figure 13.

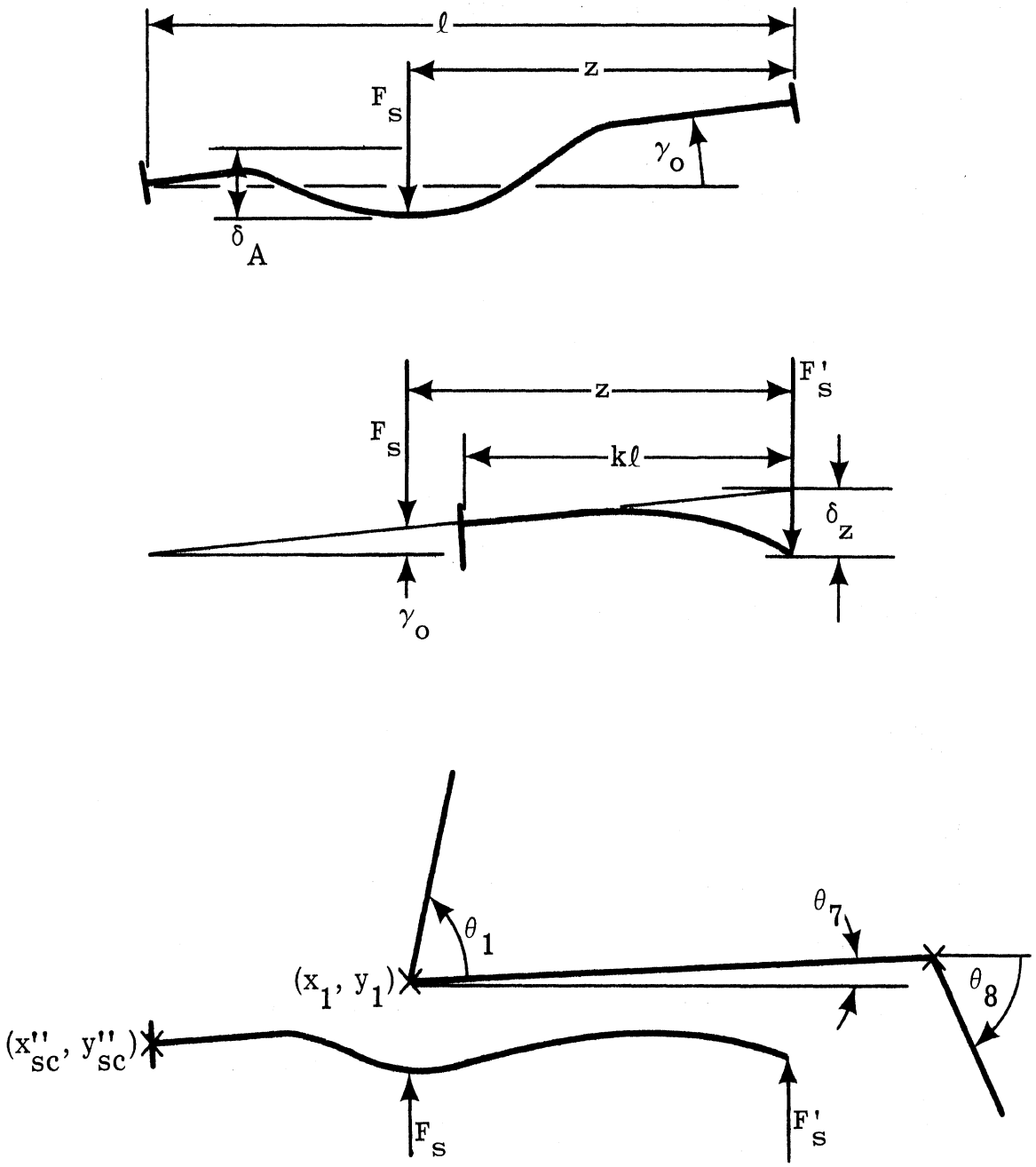

Figure 13

NON-RIGID BEAM SEAT GEOMETRY

The flow diagram is shown in figure 14, and auxiliary variables and parameters are calculated from the following equations:

$$z(t) = z_o - x_1(t),$$

$$a = \ell - z(t),$$

$$b = z^3(t) - 3k^2\ell^2 z(t) + 2k^3\ell^3,$$

$$c = k\ell - z(t),$$

$$d = y''_{sc} - y_1(t) + [x_1(t) - y''_{sc}] \tan \gamma_o,$$

$$\alpha_L = \sin^{-1}\left(\frac{r_1 - r_7}{L_7}\right),$$

$$\alpha_\ell = \sin^{-1}\left(\frac{r_7 - r_a}{L_8}\right),$$

$$\delta_A = r_1 + d,$$

$$F^* = \frac{e_1\ell^3\delta_A}{a^3z^3(t)}, \quad F^*_s = \frac{e_2\delta_z}{k^3\ell^3}, \quad \hat{F} = \frac{e_1 b\delta_z}{2k^3a^3z^3(t)}, \quad \hat{F}_s = \frac{2e_2k\ell\delta_A}{bc}.$$

Body parameters involved are the hip radius r_1, knee radius r_7, and backward ankle radius r_a. Beam parameters, besides the lengths mentioned, are e_1 and e_2, where e is twice the product of the moment of inertia and the Young's modulus for the beam.

Energy calculations must be done incrementally as for the belt and contact forces.

There are two reasons why this representation has not been incorporated into the simulation. The first is that, since the seat forces are no longer derived from the potential energy, the body

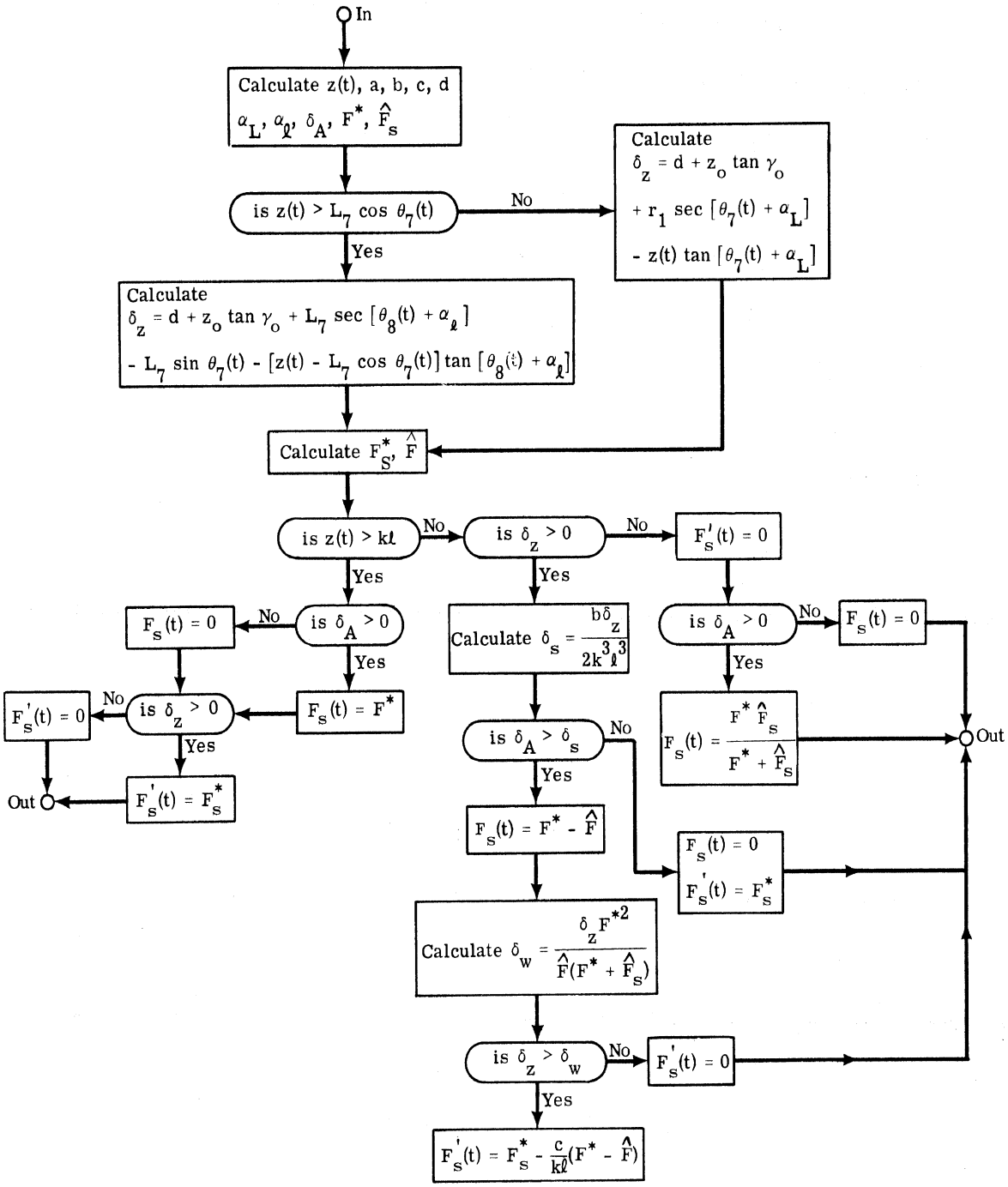

Figure 14

NON-RIGID BEAM SEAT FORCES FLOW DIAGRAM

equations would have to be re-derived. The second is that experimental confirmation and numerical data are as yet lacking.

A second possible alternate representation for the seat cushion is that of a rigid beam with some mass and inertia supported by a linear spring at the front edge and by a nonlinear spring plus damper somewhere near the other end. Figure 15 shows the geometry and relevant parameters. It is assumed that the horizontal location of the seat center of gravity remains fixed at about half its projected length. Additional parameters needed in this case are the unloaded seat cushion angle (γ_u) and the unloaded y-coordinate of the seat center of gravity (y_{gu}), as well as its mass (m_s), moment of inertia (I_s), and the distances of the center of mass and spring-damper support from the front edge (a' and a respectively).

The representation, however, requires two additional degrees of freedom - those of the y-coordinates of the seat center of gravity and of its angle to the horizontal. These two accelerations can be found in terms of the seat support forces, some parameters, and $z(t)$ and $y_1(t)$, so that they are at least uncoupled from the matrix equation and may be solved for independently.

The equations are:

$$m_s \ddot{y}_g(t) = F_s(t) + F'_s(t) - W_o - \hat{F}'_{so} - m_s g + m_s \ddot{y}_1(t)$$

$$I_s \ddot{\gamma}(t) = a'[F'_s(t) - \hat{F}'_{so}] + (a'-a)F_s(t) + W_o[z(t)-a]$$

$$F_s(t) = \sum_{m=1}^{3} \beta_m \Delta_s^m(t) + c_s \dot{\Delta}_s(t)$$

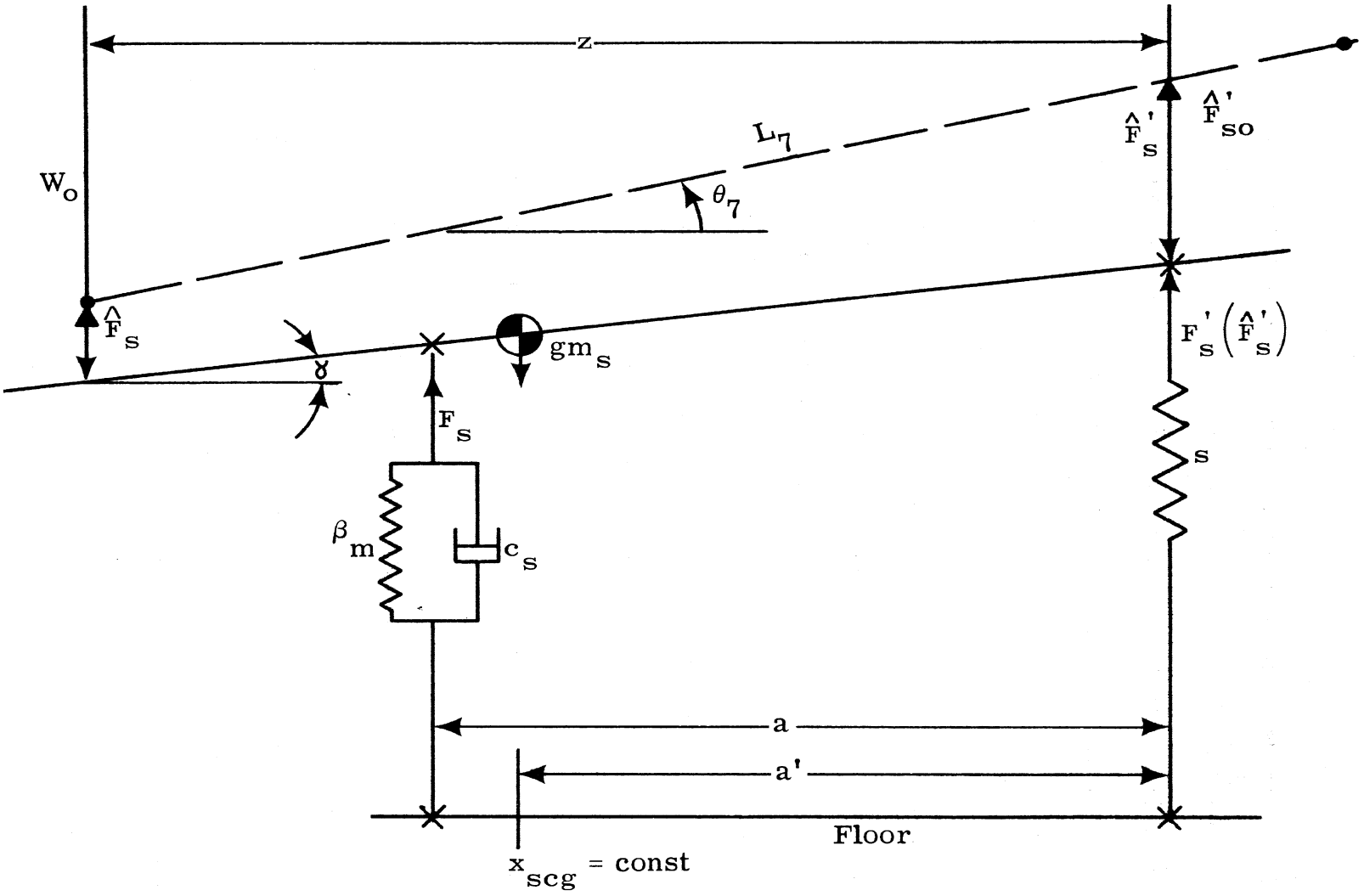

Figure 15

RIGID BEAM SEAT GEOMETRY

$$F'_s(t) = s\Delta_z(t)$$

$$\Delta_s(t) = y_{gu} - y_g(t) + (a-a')[\tan\gamma(t)-\tan\gamma_u]$$

$$\Delta_z(t) = y_{gu} - y_g(t) + a'[\tan\gamma_u-\tan\gamma(t)]$$

$$\dot{\Delta}_s(t) = (a-a')\dot{\gamma}(t)\sec^2\gamma(t) - \dot{y}_g(t)$$

The first two determine the accelerations; the last five the seat support forces (F_s and F'_s) in terms of $y_g(t)$, $\dot{y}_g(t)$, $\gamma(t)$, $\dot{\gamma}(t)$ and the parameters of the seat (β_m, c_s, s; a, a', y_{gu}, γ_u). At time t=0 there are six initial conditions (F_{so}, F'_{so}, Δ_{so}, Δ_{zo}, γ_o, y_{go}) as well as z_o, and parameters (w_o, $\hat{F}'_{so}$, I_s, m_s), while all velocities and accelerations are zero. Thus there are six operative equations (all except the last, which is satisfied trivially). Usually z_o, I_s, m_s, y_{gu}, γ_u, s, c_s, and the β_m can be measured and then any four of the remaining ten (a, a', w_o, $\hat{F}'_{so}$, F_{so}, F'_{so}, Δ_{so}, Δ_{zo}, y_{go}, γ_o) will determine the other six.

Figure 16 shows the flow diagram for determining the forces on the body in terms of the seat support forces.

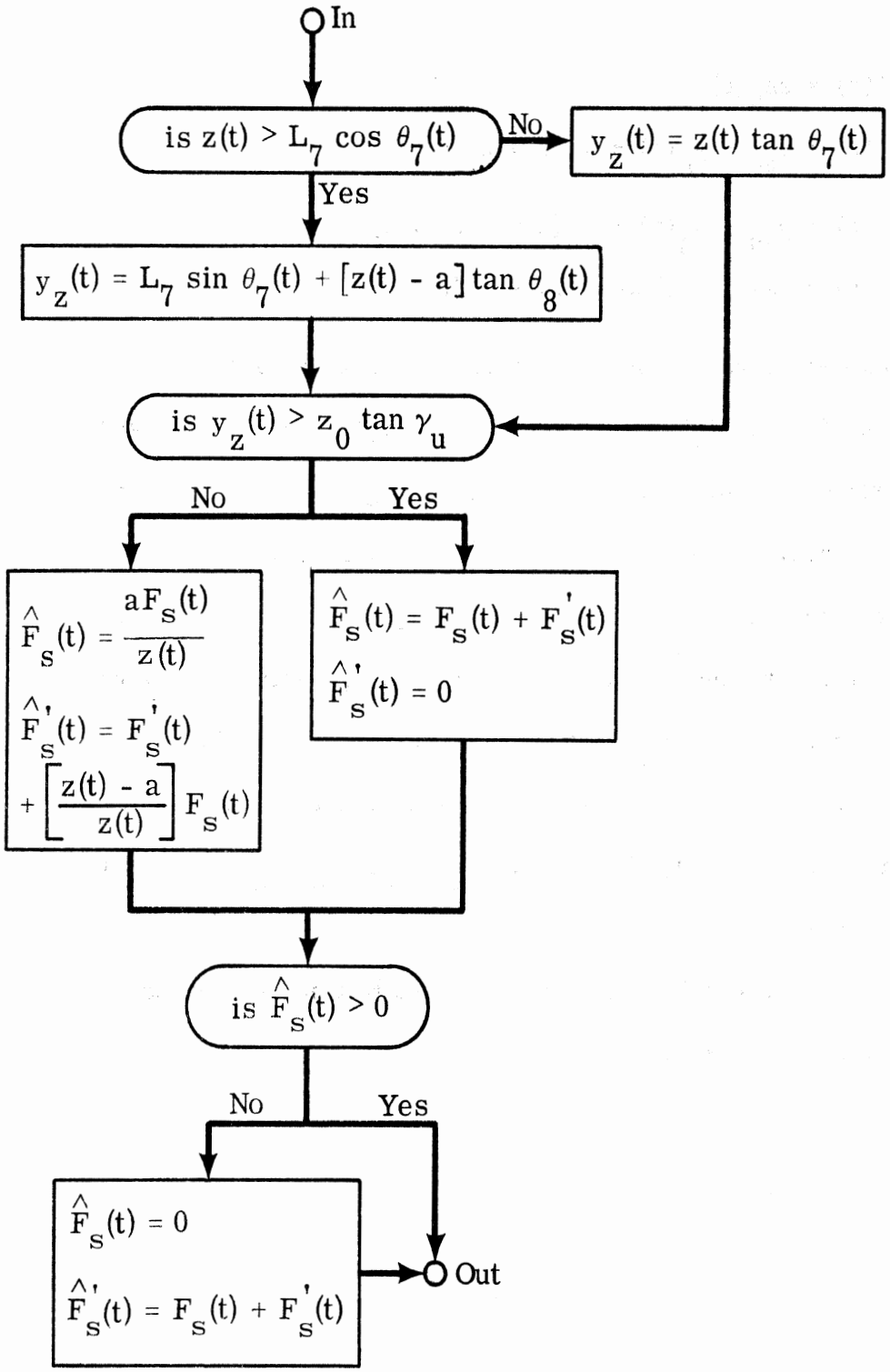

Figure 16

RIGID BEAM SEAT FORCES FLOW DIAGRAM

SECTION C.4.e

BELT FORCES

The restraint system consists of a lap belt and a diagonal torso restraint. Logic in the program allows the simulation of both belts, of neither belt, or of either one of them singly.

Each belt's nominal deformation and rate is computed from its geometry and the present state of the system. But the nominal deformation is the sum of the actual belt elongation and the body deflection. For the lap belt the latter occurs in the abdomen; for the torso restraint in the chest. Thus the total deformation must be partitioned between the belt elongation and the body deflection, and likewise for the rate. Once the actual belt elongations and rates have been obtained, they may be used to find the belt load forces, which in turn determine the generalized forces. Recurrent loading with additive residual elongation is allowed. Figure 17 shows the lap belt geometry. The geometric equations for the nominal deformation and rate are, for the lap belt (j=1):

$$\phi_1(t) = \sin^{-1}\frac{h_1}{\sqrt{u_1^2(t)+v_1^2(t)}} + \tan^{-1}\left[\frac{v_1(t)}{u_1(t)}\right],$$

$$\delta_1(t) = \sqrt{u_1^2(t) + v_1^2(t) - h_1^2} - \ell_{1o} + h_1[\phi_1(t)-\theta_1(t)+\tfrac{1}{2}\pi],$$

$$\dot{\delta}_1(t) = \dot{x}_1(t)\cos\phi_1(t) + \dot{y}_1(t)\sin\phi_1(t) - h_1\dot{\theta}_1(t),$$

where $u_1(t)=x_1(t)+\lambda_1$ and $v_1(t)=y_1(t)+\lambda_2$. For the torso restraint (j=2,3), the equations are:

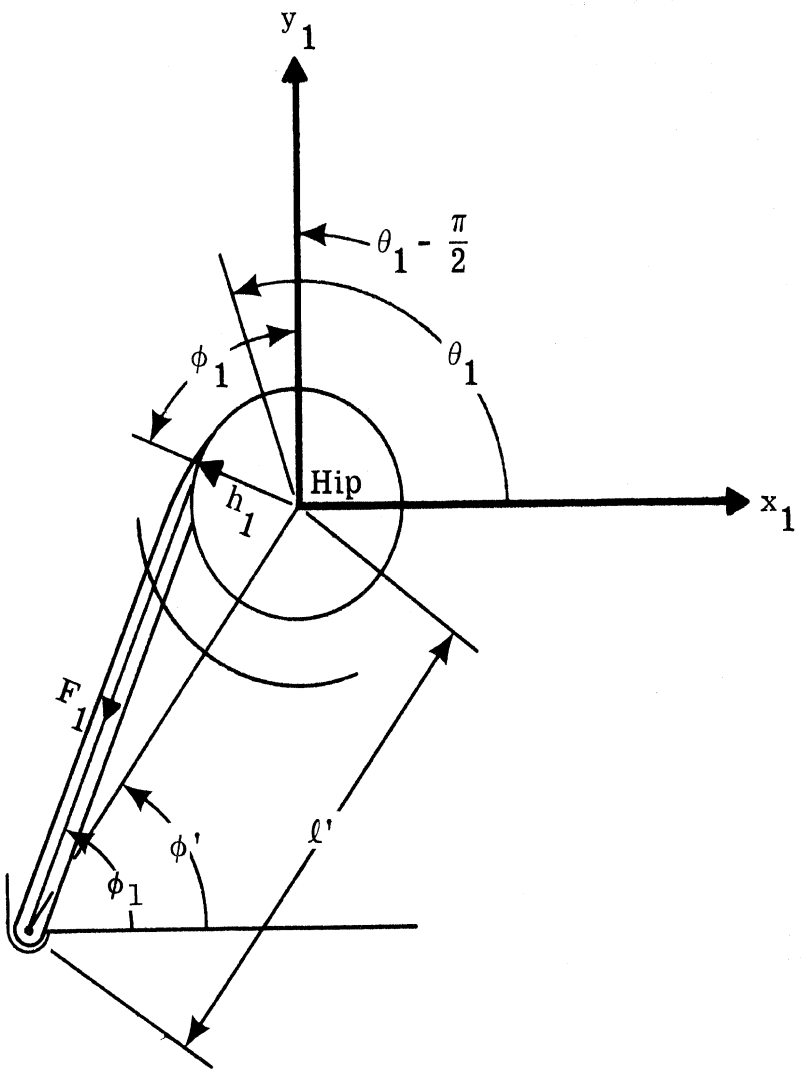

Figure 17

LAP BELT GEOMETRY

$$\phi_j(t) = \tan^{-1}\left[\frac{v_j(t)}{u_j(t)}\right],$$

$$\delta_j(t) = \sqrt{u_j^2(t) + v_j^2(t)} - \ell_{jo},$$

$$\dot{\delta}_j(t) = \dot{x}_j(t)\cos\phi_j(t) + \dot{y}_j(t)\sin\phi_j(t) + h_j\dot{\theta}_j(t)\sin[\phi_j(t)-\theta_j(t)];$$

where

$$u_2(t) = x_2(t) + h_2\cos\theta_2(t) - \lambda_3,$$

$$v_2(t) = y_2(t) + h_2\sin\theta_2(t) - \lambda_4,$$

$$u_3(t) = x_3(t) + h_3\cos\theta_3(t) - \lambda_5,$$

$$v_3(t) = y_3(t) + h_3\sin\theta_3(t) - \lambda_6.$$

The $x_i(t)$, $y_i(t)$ were calculated at the beginning of section C.4 and the λ_i in section C.2.

Details of recurrent loading are shown in figure 18 and the flow diagram for the belt forces in figure 19. There are essentially two types of recurrent loading, one in which the load is completely removed before the new loading cycle begins and the other in which it is not. The former is marked case 1 in figure 18 and the latter case 2. In both cases the new cycle begins at the point marked x, where $\dot{\delta}(t)$ equals zero, going from negative to positive. The residual or permanent deformation for the new cycle (ε_{n+1}) is calculated differently in the two cases.

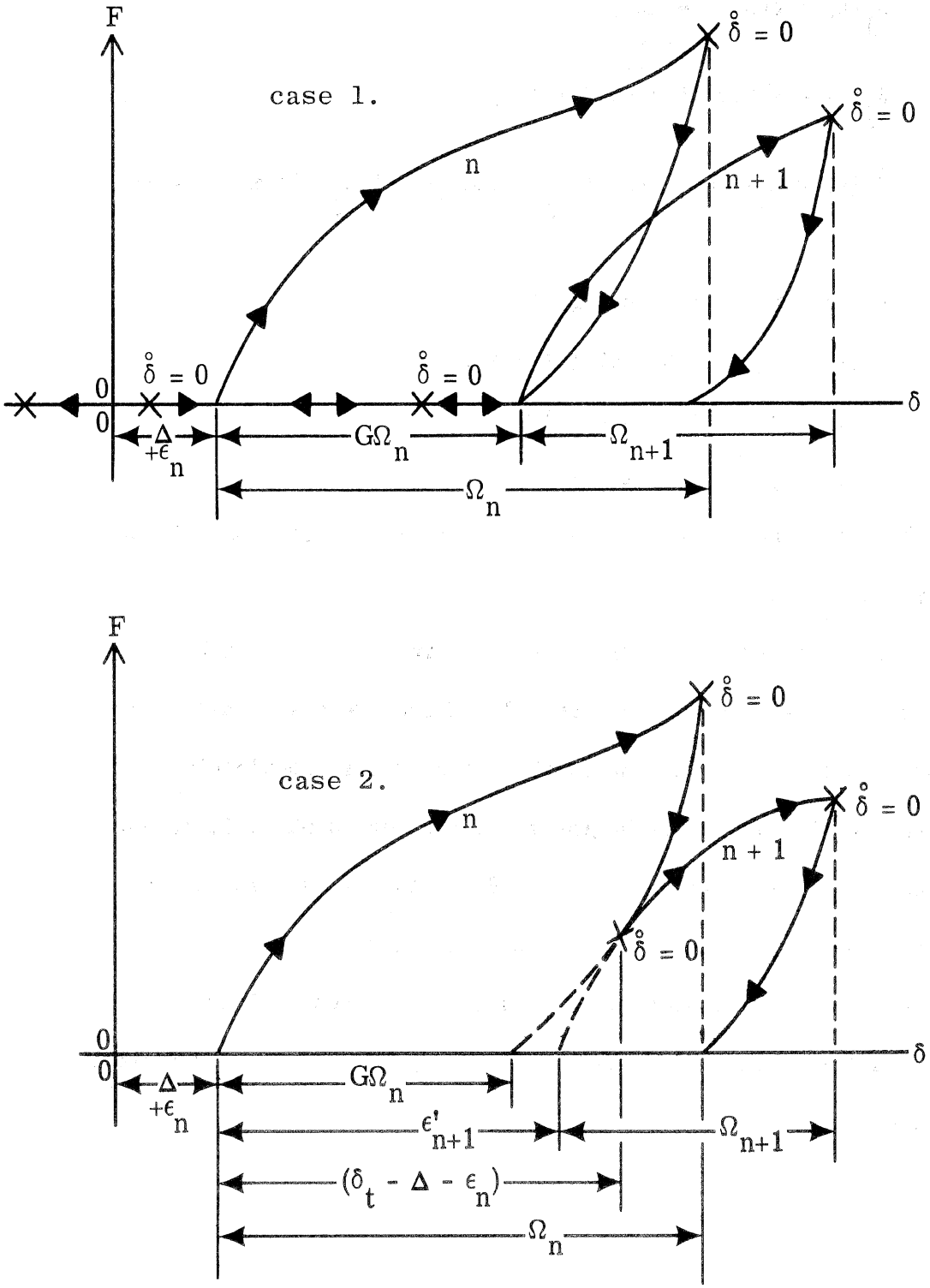

Figure 18

RECURRENT LOADING CURVES

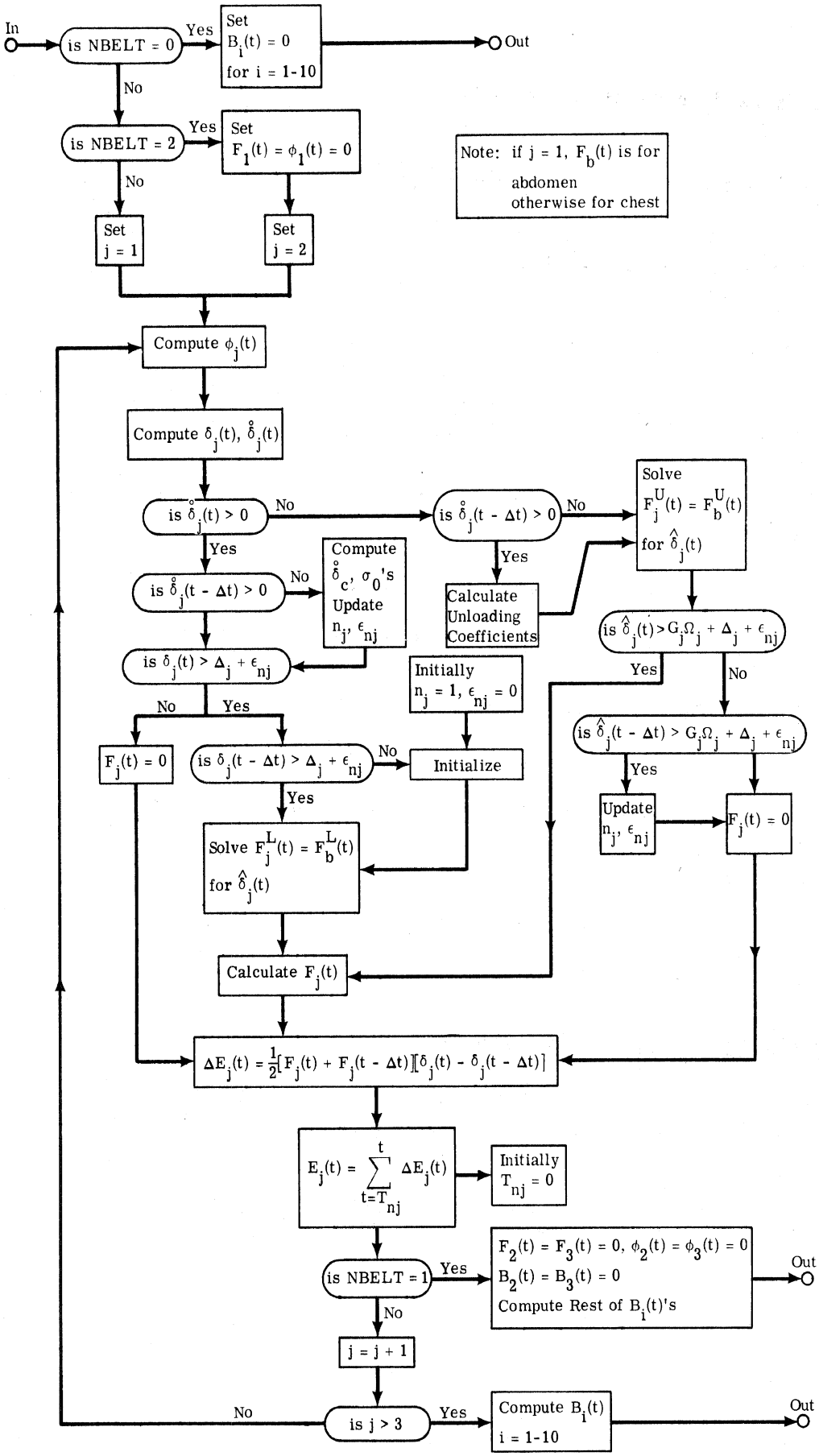

Figure 19

BELT FORCE FLOW DIAGRAM

The generalized force relations are:

$$B_1(t) = h_1 F_1(t) + L_1 \sum_{j=2}^{3} F_j(t)\sin[\theta_1(t)-\phi_j(t)],$$

$$B_i(t) = \sum_{j=i}^{3} h_j F_j(t)\sin[\theta_i(t)-\phi_j(t)] \quad \text{for } i=2,3,$$

$$B_i(t) = 0 \quad \text{for } i=4-8,$$

$$B_9(t) = -\sum_{j=1}^{3} F_j(t)\cos[\phi_j(t)- \Phi(t_m)],$$

$$B_{10}(t) = -\sum_{j=1}^{3} F_j(t)\sin[\phi_j(t)-\Phi(t_m)].$$

It may prove necessary to modify the lap belt calculations so as to include both sides explicitely, rather than regarding them as identical. The reason would be that the left and right hand side anchorage locations in actual cars do not have the same coordinates. If this is so, then the initial belt length and angle would be different for the two sides. If these differences are small, it may be possible to neglect them and either average the two sides or use one of them consistently.

SECTION C.4.f

CONTACT FORCES

The contact surfaces considered are both sides of the head rest and seat back, the roof, windshield, sun visor, upper and lower instrument panels, floor and toeboard, and steering wheel rim and column. All of these except the head rest, sun visor, and steering wheel are assumed to be rigidly fixed relative to the interior of the vehicle. It is further assumed that the characteristics of the motion and material of the nonrigid surfaces can be lumped, with the exception of the column which may be padded. In this latter case, it is assumed that the column does not move until its padding (if any) has bottomed out. These assumptions simplify the calculations a great deal and are sufficiently realistic.

In this present simulation, the nonrigid contact surfaces are characterized by load-deflection relations rather than by explicit differential equations. The latter is a better and more accurate representation, but requires that the number of degrees of freedom of the system be raised by approximately six, since the rim and column would need at least two degrees of freedom each and the head rest and sun visor one. This will be done in phase three.

Figure 20 shows the overall contact force flow diagram; its more complicated parts are defined in figures 22 to 24 and in tables 7 to 11.

The body reference point coordinates and their velocities are calculated from the following equations, referred to in figure 20 as

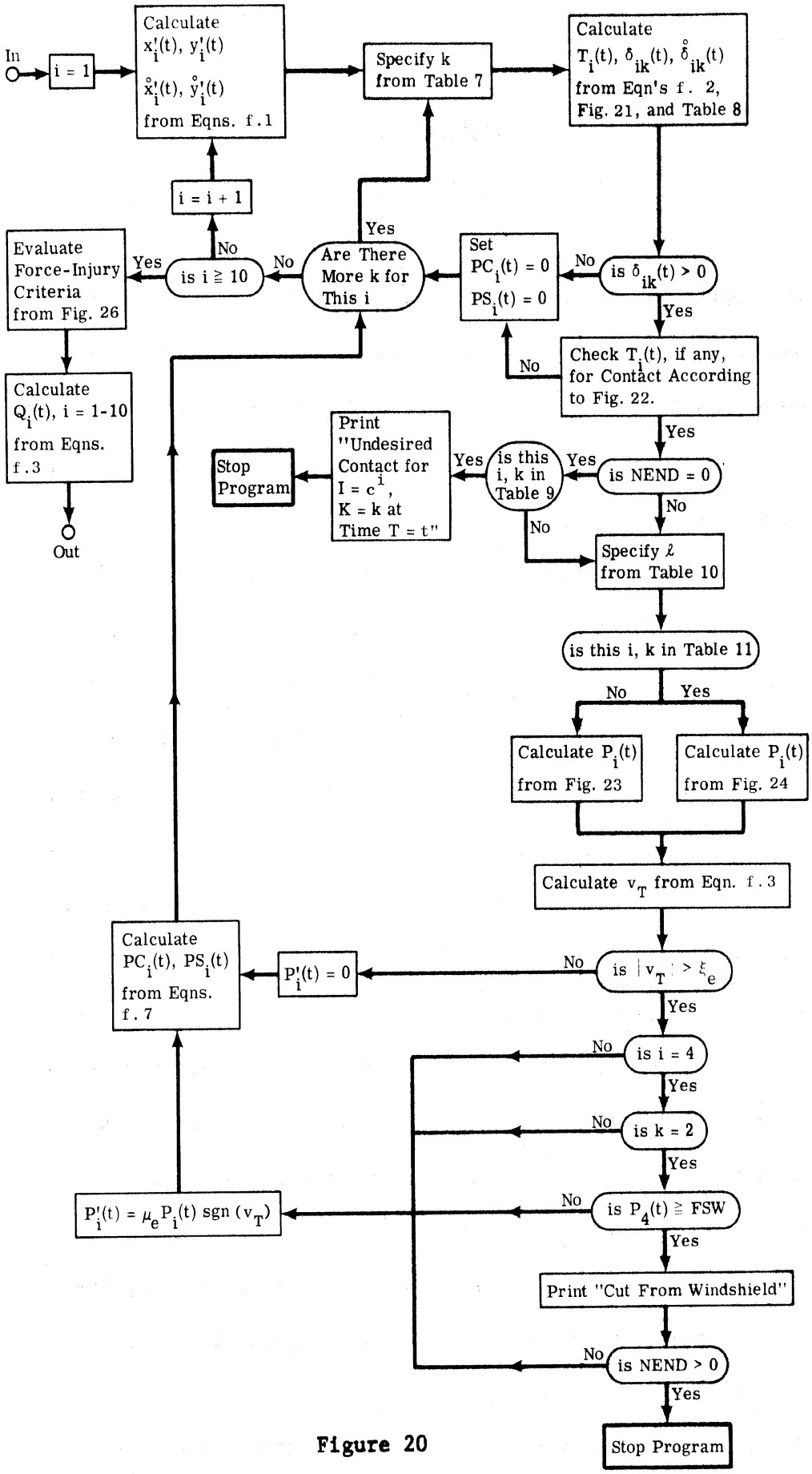

Figure 20

CONTACT FORCE FLOW DIAGRAM

equations f.1.

i=1,5, 6,7:	$x_i'(t) = x_i(t)$	$\dot{x}_i'(t) = \dot{x}_i(t)$
	$y_i'(t) = y_i(t)$	$\dot{y}_i''(t) = \dot{y}_i(t)$
i=2,3:	$x_i'(t)=x_3(t)+\rho_i'\cos[\theta_3(t)+\gamma_i]$	$\dot{x}_i'(t)=\dot{x}_3(t)-\rho_i'\dot{\theta}_3(t)\sin[\theta_3(t)+\gamma_i]$
	$y_i'(t)=y_3(t)+\rho_i'\sin[\theta_3(t)+\gamma_i]$	$\dot{y}_i'(t)=\dot{y}_3(t)+\rho_i'\dot{\theta}_3(t)\cos[\theta_3(t)+\gamma_i]$
i=4:	$x_4'(t) = x_4(t)+\rho_4\cos\theta_4(t)$	$\dot{x}_4'(t)=\dot{x}_4(t)-\rho_4\dot{\theta}_4(t)\sin\theta_4(t)$
	$y_4'(t) = y_4(t)+\rho_4\sin\theta_4(t)$	$\dot{y}_4'(t)=\dot{y}_4(t)+\rho_4\dot{\theta}_4(t)\cos\theta_4(t)$
i=8:	$x_8'(t)=x_7(t)+L_8\cos\theta_8(t)$	$\dot{x}_8'(t)=\dot{x}_7(t)-L_8\dot{\theta}_8(t)\sin\theta_8(t)$
	$y_8'(t)=y_7(t)+L_8\sin\theta_8(t)$	$\dot{y}_8'(t)=\dot{y}_7(t)+L_8\dot{\theta}_8(t)\cos\theta_8(t)$
i=9:	$x_9'(t) = x_7(t)$	$\dot{x}_9'(t) = \dot{x}_7(t)$
	$y_9'(t) = y_7(t)$	$\dot{y}_9'(t) = \dot{y}_7(t)$
i=10:	$x_{10}'(t)=x_6(t)+L_6\cos\theta_6(t)$	$\dot{x}_{10}'(t)=\dot{x}_6(t)-L_6\dot{\theta}_6(t)\sin\theta_6(t)$
	$y_{10}'(t)=y_6(t)+L_6\sin\theta_6(t)$	$\dot{y}_{10}'(t)=\dot{y}_6(t)+L_6\dot{\theta}_6(t)\cos\theta_6(t)$

Table 7 shows what surfaces can be contacted by which body segments for the three occupant positions.

Body Segment	Subscript i	subscript k: Driver	Front-Seat Passenger	Rear-Seat Passenger
hip	1	9	9	9*
back	2	9	9	9*
chest	3	8,10	4	7
head	4	1,2,3,8,9,10,11	1,2,3,4,9,11	1,7,9*,11,1*
shoulder	5	10	-	-
elbow	6	9	9	9*
knee	7	5	5	7
foot	8	6,12	5,6,12	6*,7,12*
shin	9	5*	5*	-
hand	10	5,10*,11	4,5,11	7,11

where 1* indicates the back of the front-seat head rest, 5* the lower edge of the lower panel,6* the sloping section of the rear-seat floor, 9* the rear-seat back, 10* the side rim of the steering wheel, and 12* the rear-seat floor.

TABLE 7.

Equations f.2 for $T_i(t)$, $\delta_{ik}(t)$ and $\dot{\delta}_{ik}(t)$, as derived from the various geometries shown in figure 21, are as follows:

$$\delta_{ik}(t) = r_i + [x_i'(t)-x_k'']\sin\psi_k + [y_k''-y_i'(t)]\cos\psi_k,$$

$$\dot{\delta}_{ik}(t) = \dot{y}_i'(t)\cos\psi_k - \dot{x}_i'(t)\sin\psi_k,$$

$$T_i(t) = [x_k''-x_i'(t)]\cos\psi_k + [y_k''-y_i'(t)]\sin\psi_k,$$

for the (i,k) sets of table 8, with $T_i(t)$ omitted for k=11,12. Special relations needed here are: $x_4''=x_2''-D_2\cos\psi_2$, $y_4''=y_2''-D_2\sin\psi_2$, $\psi_{10}=\psi_8$, $\psi_{11}=180°$, $y_{11}''=y_2''$, $\psi_{12}=0°$, $y_{12}''=y_6''-D_6\sin\psi_6$;

$$\delta_{ik}(t) = \frac{1}{2}D_1 + r_4 - [x_4'(t)-x_1'']\cos\gamma + [y_4'(t)-y_1'']\sin\gamma,$$

$$\dot{\delta}_{ik}(t) = \dot{x}_4'(t)\cos\gamma - \dot{y}_4'(t)\sin\gamma,$$

for i=4, k=1 and where

$$\gamma = \tan^{-1}\left[\frac{y_1''-y_4'(t)}{x_1''-x_4'(t)}\right];$$

$$\delta_{ik}(t) = r_7 - [x_5''-D_5\cos\psi_5-x_7'(t)]\sin[\theta_8(t)-\alpha_o] + [y_5''-D_5\sin\psi_5-y_7'(t)]\cos[\theta_8(t)-\alpha_o],$$

$$\dot{\delta}_{ik}(t) = \dot{y}_7'(t)\cos[\theta_8(t)-\alpha_o] - \dot{x}_7'(t)\sin[\theta_8(t)-\alpha_o] + T_9(t)\dot{\theta}_8(t),$$

$$T_i(t) = [x_5''-D_5\cos\psi_5-x_7'(t)]\cos[\theta_8(t)-\alpha_o]-[y_5''-D_5\sin\psi_5-y_7'(t)]\sin[\theta_8(t)-\alpha_o],$$

for i=9, k=5*, where α_o was defined and calculated in section C.2.

Regular (Table 8):

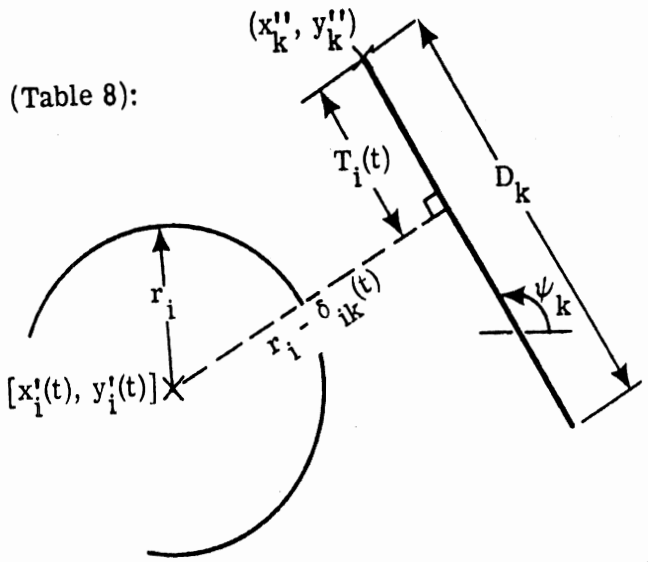

Special:

Headrest
i = 4, k = 1

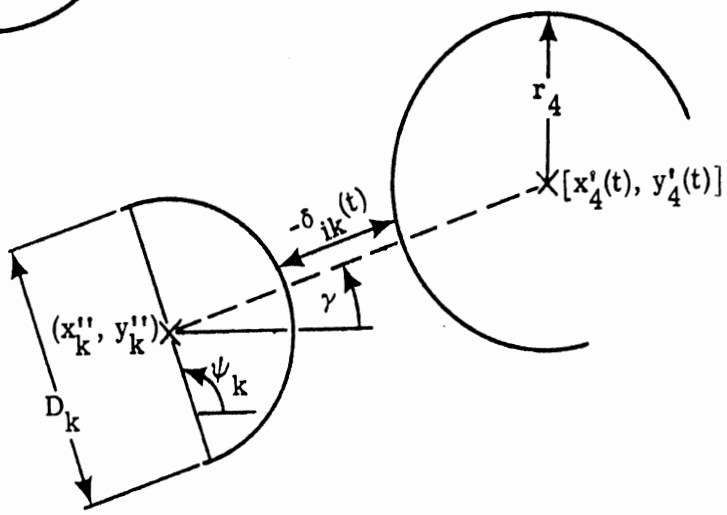

Shin
i = 9, k = 5*

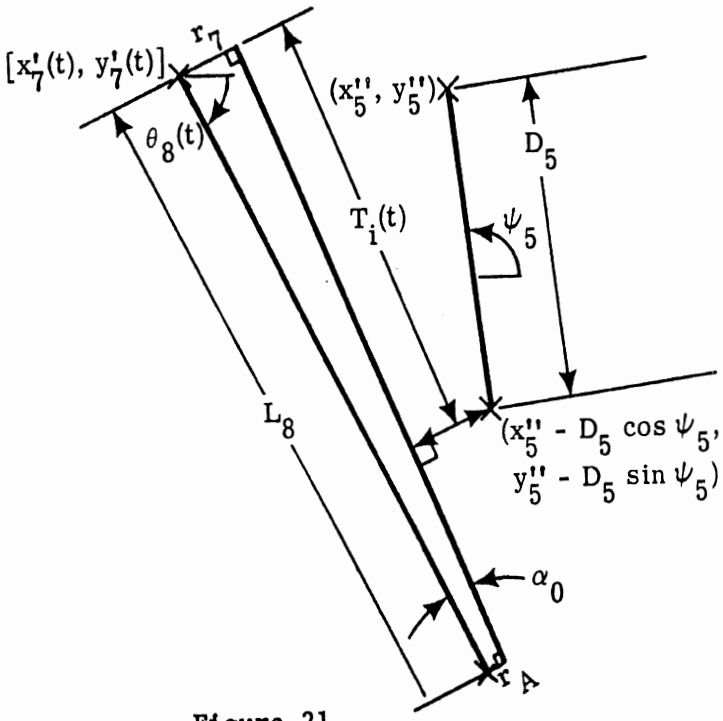

Figure 21

CONTACT GEOMETRY

subscript i	subscript k		
	Driver	Front Pass.	Rear Pass.
1	9	9	9*
2	9	9	9*
3	8,10	4	7
4	2,3,8,9,10,11	2,3,4,9,11	1*,7,9*,11
5	10*	-	-
6	9	9	9*
7	5	5	7
8	6,12	5,6,12	7,12*
10	5,10*,11	4,5,11	7,11

TABLE 8.

Figure 22 defines the $T_i(t)$ contact check and also takes care of those cases for which $T_i(t)$ is omitted.

Table 9 specifies those combinations of i and k which are termed undesirable, for use in the undesired contact end of program test.

subscript i	subscript k		
	Driver	Front Pass.	Rear Pass.
3	8,10	4	7
4	2,3,8,10,11	2,3,4,11	1*,7,11
5	10*	-	-
7	5	5	7
8	-	5	7
9	5*	5*	-
10	5,10*,11	4,5,11	7,11

TABLE 9.

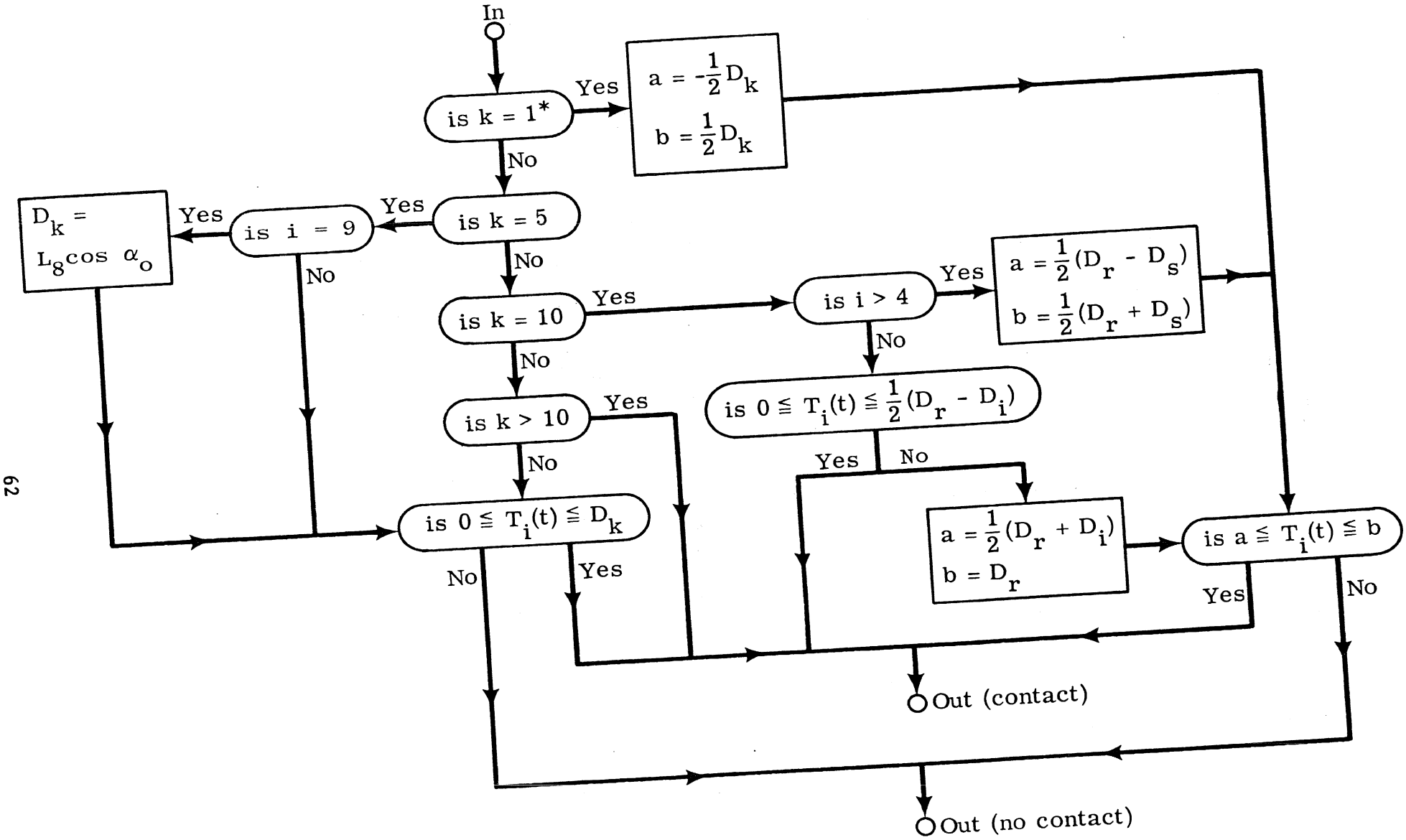

Figure 22

$T_i(t)$ CONTACT CHECK FLOW DIAGRAM

Table 10 defines, both numerically and descriptively, the composition of any particular contact surface, whether a single material, a padded surface, or a nonrigid surface.

	subscripts		
Contact Surface	k	ℓ	Composition
head rest	1	8	non-rigid motion
windshield	2	2	glass
sun visor	3	9	non-rigid motion
upper panel	4	3,6	padded metal
lower panel	5	3,6	padded metal
toeboard	6	4,5	mat on floor
back of front seat	7	1	seat material
steering column	8	3,10	padding plus non-rigid motion
seat back	9	1	seat material
steering wheel rim	10	7	non-rigid motion
roof	11	3,6	padded metal
floor	12	4,5	mat on floor

Body Segment	i	b for non-rigid motion
abdomen	1	11
chest	3	12
face	4	13
shoulder	5	14

TABLE 10.

Table 11 shows the combinations of i and k for which contact deflection is shared; i.e. deflection occurs both in the body and in the surface.

subscript	subscript k		
i	Driver	Front Pass.	Rear Pass.
3	8,10	4	7
4	8,10	4	1*,7
5	10*	-	-

TABLE 11

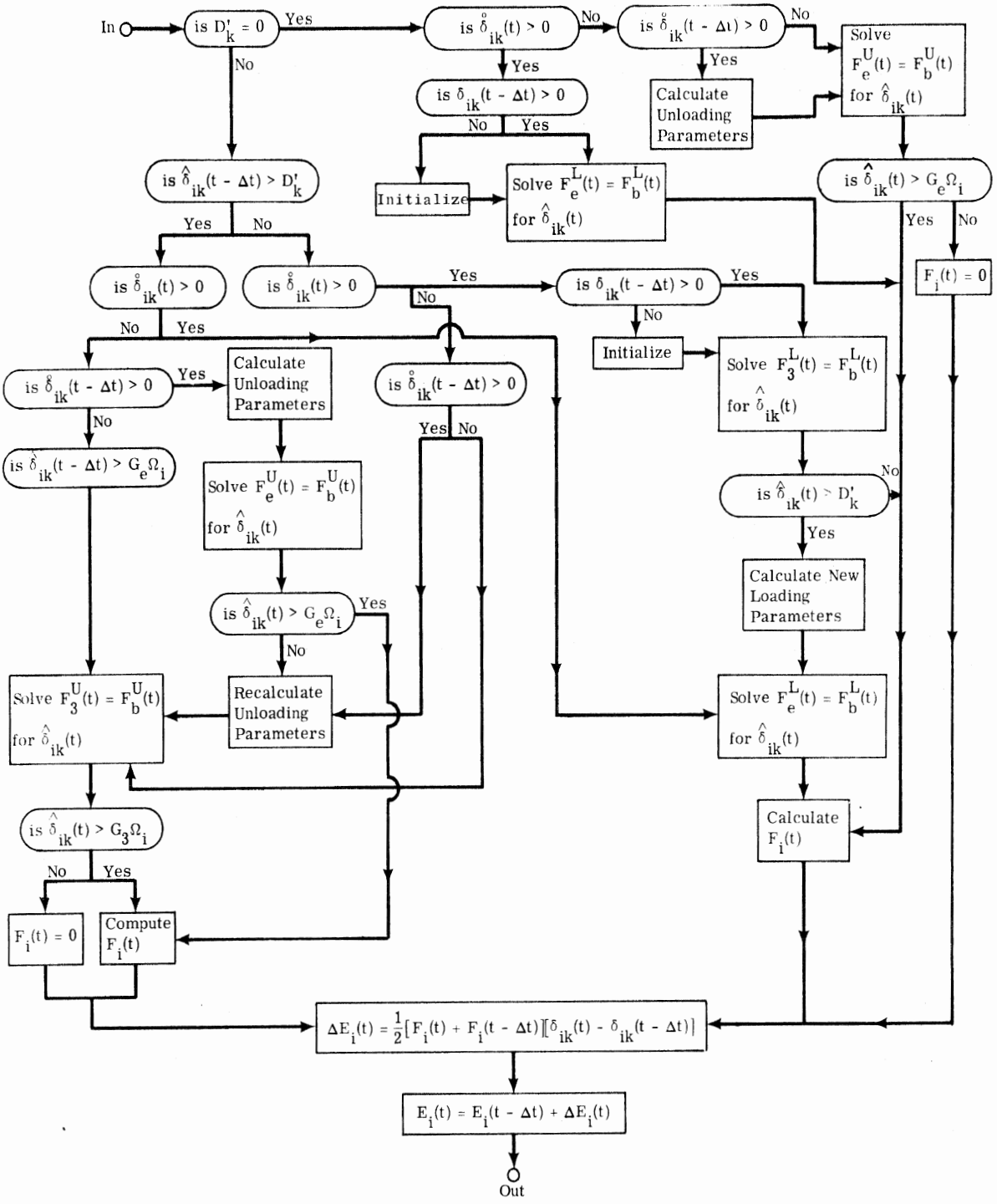

Figure 23

SHARED DEFLECTION CONTACT FORCE FLOW DIAGRAM

Figure 23 displays the flow diagram for this shared deflection force, while figure 24 contains that for deflection in or of the surface only. Figure 25 depicts a bi-material force-deflection curve.

Equations f.3 define the tangential velocity of the body along the contact surface, as follows:

$$v_T = \dot{x}'_i(t)\cos\psi_k + \dot{y}'_i(t)\sin\psi_k + r_i\dot{\theta}_i(t) \quad \text{for the Table 8 (i,k),}$$

$$v_T = \dot{y}'_4(t)\cos\gamma - \dot{x}'_4(t)\sin\gamma + r_4\dot{\theta}_4(t) \quad \text{for i=4, k=1,}$$

$$v_T = \dot{x}'_7(t)\cos[\theta_8(t)-\alpha_o] + \dot{y}'_7(t)\sin[\theta_8(t)-\alpha_o] + \delta_{97}(t)\dot{\theta}_8(t)$$
$$\text{for i=9, k=5.}$$

Equations f.4 define the present horizontal and vertical contact force components, relative to the interior of the vehicle, for each contacting body segment in terms of the normal and tangential forces and the angle of the contact surface with respect to the floor. The program also allows for the case in which one body segment contacts more than one surface at the same time, which is theoretically possible but practically unlikely. Special relations needed in these equations are: $\psi_{10}=\psi_8$, $\psi_{11}=180°$, $\psi_{12}=0°$. The proper (i,k) sets from Table 7 must be used.

$$PS_i(t) = P_i(t)\sin\psi_k + P'_i(t)\cos\psi_k$$

$$PC_i(t) = P_i(t)\cos\psi_k - P'_i(t)\sin\psi_k,$$

$$\text{i=9: } PS_9(t) = P_9(t)\sin[\alpha_o-\theta_8(t)] + P'_9(t)\cos[\alpha_o-\theta_8(t)]$$

$$PC_9(t) = P'_9(t)\sin[\theta_8(t)-\alpha_o] - P_9(t)\cos[\theta_8(t)-\alpha_o].$$

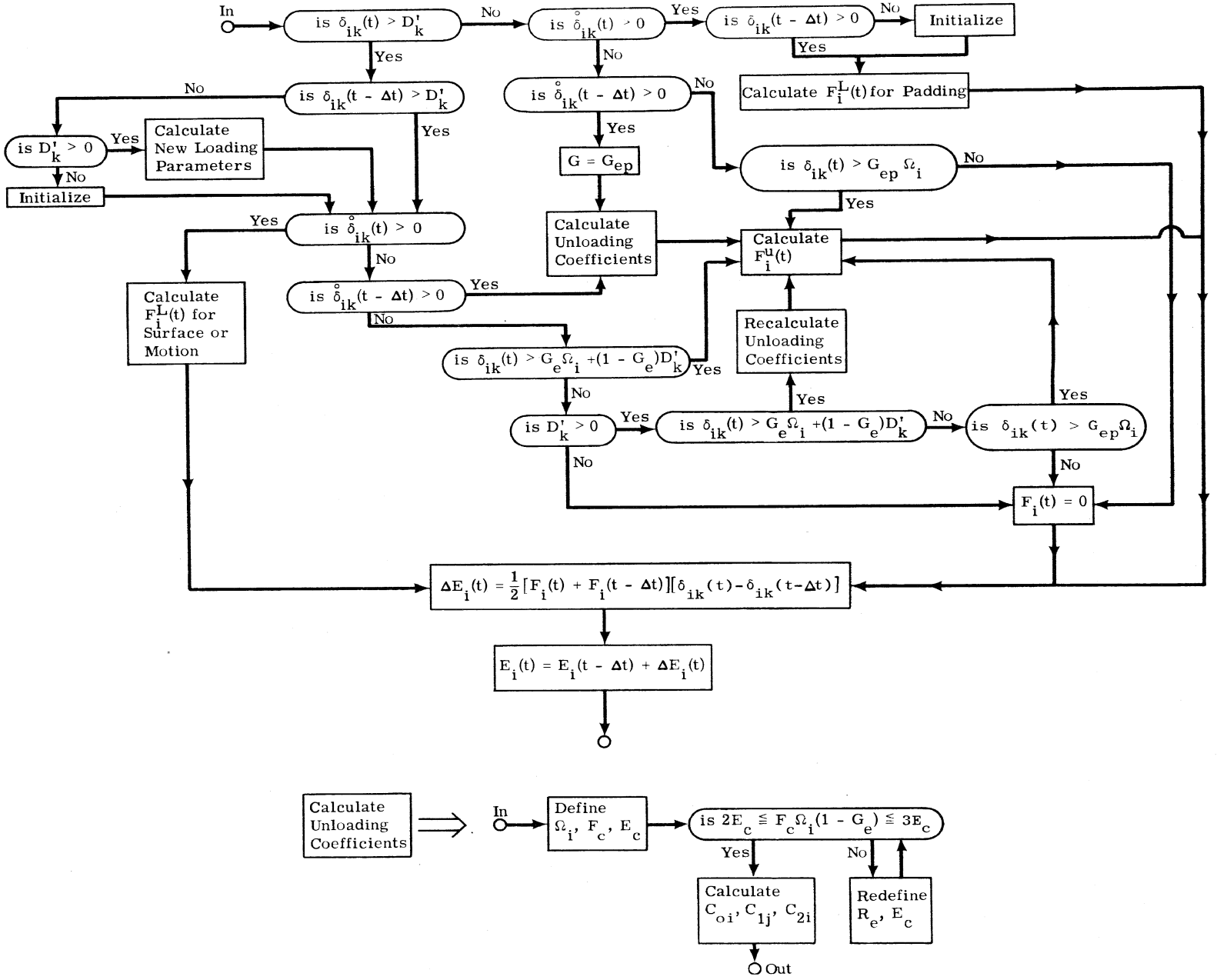

Figure 24

BI-MATERIAL CONTACT FORCE FLOW DIAGRAM

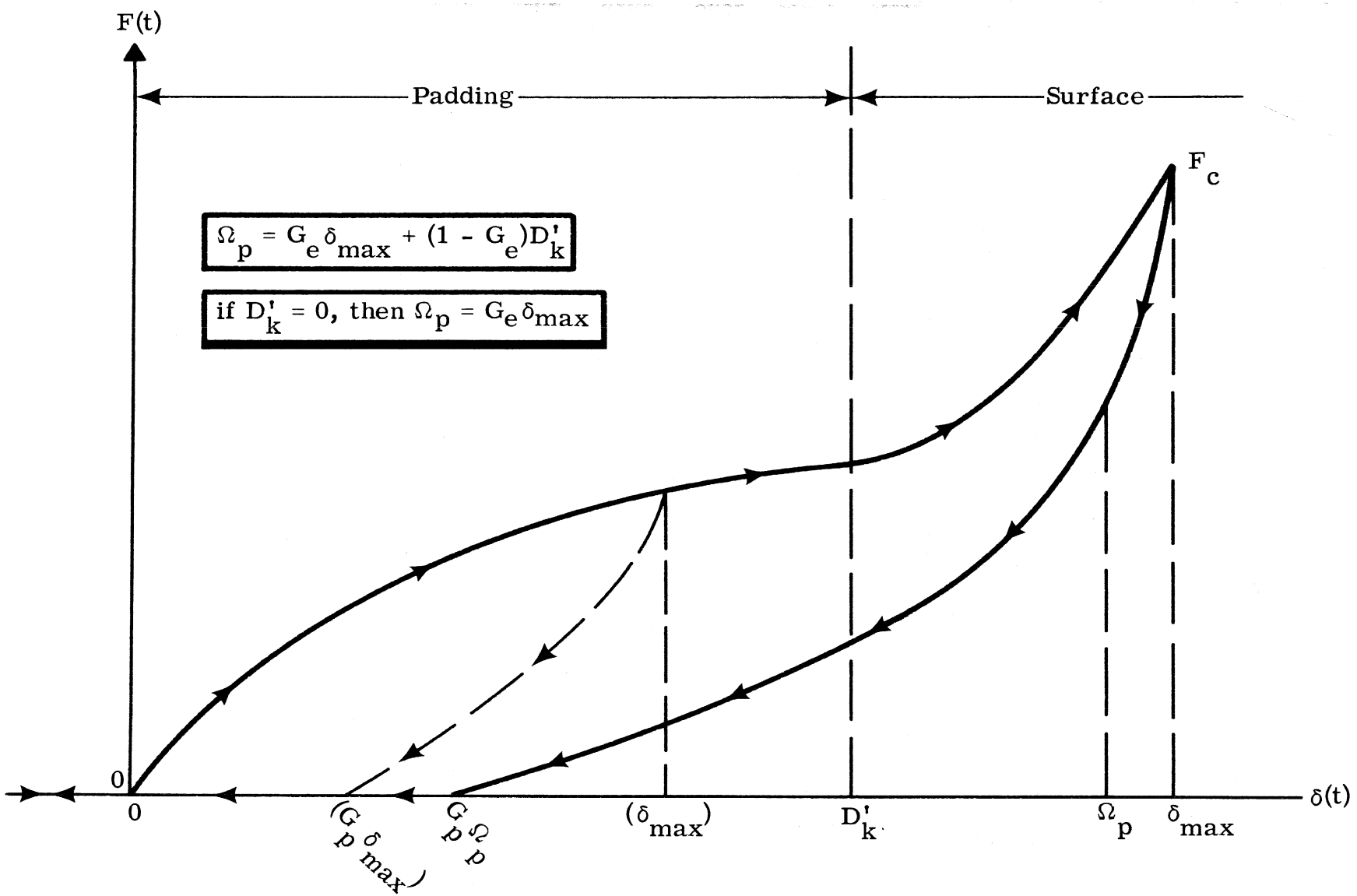

Figure 25

BI-MATERIAL LOADING CURVE

After all these contact force components have been calculated for all the contacting body segments, the three main force-based injury criteria can be evaluated. Figure 26 shows the flow diagram. These are the tension dislocations of joints and compression and shear fractures of bones. Table 5 in section C.1 shows the correspondence between the subscript i and its particular bone in each case. The forces are calculated in equations f.5, f.6, and f.7 respectively.

Equations f.5

$$FT_1 = (F_s+PC_1+PC_2+PC_4-F'_s-PC_8-PC_9)\sin\theta_1 + (f-PS_1-PS_2-PS_4-F'_s+PS_7+PS_8+PS_9)\cos\theta_1,$$

$$FT_2 = (PC_2+PC_4-F_s)\sin\theta_2 + (PS_1-PS_2-PS_4-f)\cos\theta_2 + F_3\cos(\theta_2-\phi_3) - F_2\cos(\theta_2-\phi_2),$$

$$FT_3 = (PC_4-F_s-PC_1)\sin\theta_3 + (PS_1-f-PS_7)\cos\theta_3 + F_2\cos(\theta_3-\phi_2) + F_3\cos(\theta_3-\phi_3),$$

$$FT_4 = (PC_4-F_s-PC_1-PC_2)\sin\theta_4 + (PS_1+PS_2-f-PS_4)\cos\theta_4 + F_2\cos(\theta_4-\phi_2) - F_1\cos(\theta_4-\phi_1) - F_3\cos(\theta_4-\phi_3),$$

$$FT_5 = (PC_5+PC_6+PC_{10}-F_s-PC_1-PC_2-PC_4)\sin\theta_5 - F_1\cos(\theta_5-\phi_1) + (PS_1+PS_2+PS_4-f-PS_5-PS_6-PS_{10})\cos\theta_5 + F_2\cos(\theta_5-\phi_2) - F_3\cos(\theta_5-\phi_3),$$

$$FT_6 = (PC_6+PC_{10}-PC_2-PC_5)\sin\theta_6 + (PS_2+PS_5-PS_6-PS_{10})\cos\theta_6,$$

$$FT_7 = (PC_7+PC_8+PC_9-F_s-F'_s)\sin\theta_8 + (PS_1-f-F'_s-PS_7-PS_8-PS_9)\cos\theta_8.$$

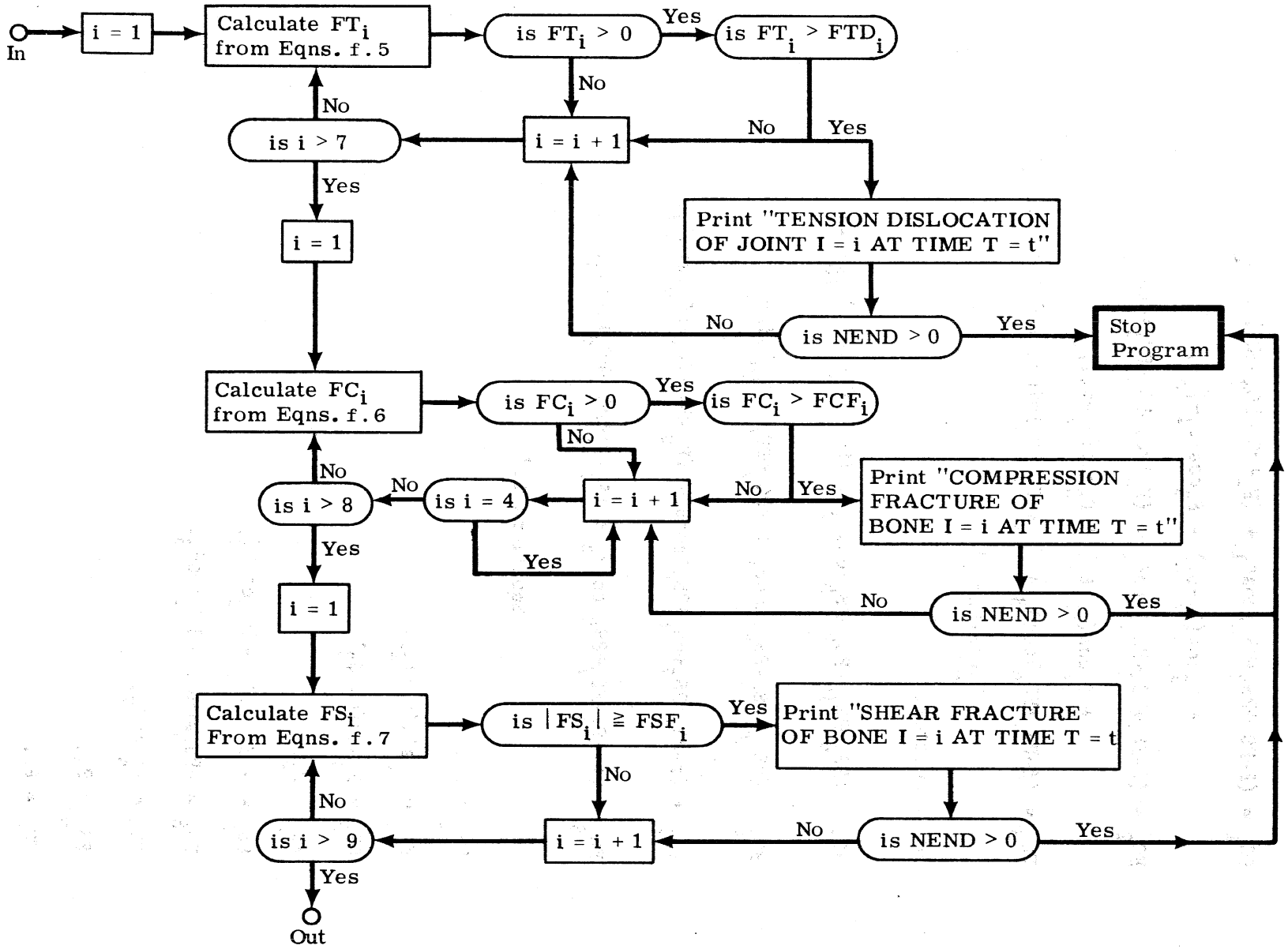

Figure 26

FORCE-INJURY CRITERIA FLOW DIAGRAM

Equations f.6

$$FC_1 = (f-PS_1+PS_2+PS_4)\cos\theta_1 + (F_s+PC_1-PC_2-PC_4)\sin\theta_1 + F_2\cos(\theta_1-\phi_2) - F_3\cos(\theta_1-\phi_3),$$

$$FC_2 = (f-PS_1+PS_2+PS_4)\cos\theta_2 + (F_s+PC_1-PC_2-PC_4)\sin\theta_2 + F_1\cos(\theta_2-\theta_1) + F_3\cos(\theta_2-\phi_3),$$

$$FC_3 = (f-PS_1+PS_4)\cos\theta_3 + (F_s+PC_1-PC_4)\sin\theta_3 + F_1\cos(\theta_1-\theta_3) - F_2\cos(\theta_3-\phi_2),$$

FC_4 omitted,

$$FC_5 = (PS_6+PS_{10}-PS_2-PS_5)\cos\theta_5 + (PC_2+PC_5-PC_6-PC_{10})\sin\theta_5,$$

$$FC_6 = (PS_{10}-PS_5-PS_6)\cos\theta_6 + (PC_5+PC_6-PC_{10})\sin\theta_6,$$

$$FC_7 = (f-PS_1+PS_7+PS_8+PS_9)\cos\theta_7 + (F_s-PC_7-PC_8-PC_9)\sin\theta_7,$$

$$FC_8 = (f-PS_1-PS_7+PS_8)\cos\theta_8 + (F_s+F'_s+PC_7-PC_8)\sin\theta_8.$$

Equations f.7

$$FS_1 = F_1,$$

$$FS_2 = F_2\sin(\theta_2-\phi_2),$$

$$FS_3 = F_3\sin(\theta_3-\phi_3),$$

$$FS_4 = P_4,$$

$$FS_5 = -PS_2\sin\theta_3 - PC_2\cos\theta_3,$$

$$FS_6 = -PS_3\sin\theta_3 - PC_3\cos\theta_3,$$

$$FS_7 = F'_s\cos\theta_7,$$

$$FS_8 = P_9,$$

$$FS_9 = P_7.$$

Finally the contact generalized forces are calculated from Equations f.8, as follows:

$$Q_1(t) = L_1[\sin\theta_1(t) \sum_{i=1}^{6,10} PS_i(t) + \cos\theta_1(t) \sum_{i=1}^{6,10} PC_i(t)] - r_1 P_1'(t),$$

$$Q_2(t) = L_2[\sin\theta_2(t) \sum_{i=2}^{6,10} PS_i(t) + \cos\theta_2(t) \sum_{i=2}^{6,10} PC_i(t)],$$

$$Q_3(t) = L_3[PS_4(t)\sin\theta_3(t) + PC_4(t)\cos\theta_3(t)] - r_2 P_2'(t) - r_3 P_3'(t)$$
$$+ L_4[\sin\theta_3(t) \sum_{i=5}^{6,10} PS_i(t) + \cos\theta_3(t) \sum_{i=5}^{6,10} PC_i(t)]$$
$$+ \sum_{i=2}^{3} \rho_i'\{PS_i(t)\sin[\theta_i(t)+\gamma_i] + PC_i(t)\cos[\theta_3(t)+\gamma_i]\},$$

$$Q_4(t) = \rho_4'[PS_4(t)\sin\theta_4(t) + PC_4(t)\cos\theta_4(t)] - r_4 P_4'(t),$$

$$Q_5(t) = L_5[\sin\theta_5(t) \sum_{i=5}^{6,10} PS_i(t) + \cos\theta_5(t) \sum_{i=5}^{6,10} PC_i(t)] - r_5 P_5'(t) - r_6 P_6'(t),$$

$$Q_6(t) = L_6[PS_{10}(t)\sin\theta_6(t) + PC_{10}(t)\cos\theta_6(t)] - r_{10} P_{10}'(t),$$

$$Q_7(t) = L_7[\sin\theta_7(t) \sum_{i=7}^{9} PS_i(t) + \cos\theta_7(t) \sum_{i=7}^{9} PC_i(t)] - r_7 P_7'(t),$$

$$Q_8(t) = L_8[PS_8(t)\sin\theta_8(t) + PC_8(t)\cos\theta_8(t)] - r_8 P_8'(t) - r_7 P_9'(t) - T_9(t) P_9(t),$$

$$Q_9(t) = \sum_{i=1}^{10} [PC_i(t)\sin\Phi(t_m) - PS_i(t)\cos\Phi(t_m)],$$

$$Q_{10}(t) = \sum_{i=1}^{10} [PS_i(t)\sin\Phi(t_m) + PC_i(t)\cos\Phi(t_m)].$$

SECTION C.5

ACCELERATIONS

In the present simulation, the vehicle accelerations are read from tables. These include the horizontal and vertical accelerations of the vehicle center of gravity and its pitch acceleration.

The accelerations of the generalized coordinates for the body are found by inverting the matrix equation $A\ddot{\vec{z}} = \vec{b}$ and solving. The vector $\vec{b}$ has already been computed in Section C.4. The matrix A is shown in figure 27, where the a_i were defined and computed in Section C.2.

$$
A = \begin{bmatrix}
a_{10} & a_2L_1\cos(\Theta_1-\Theta_2) & a_3L_1\cos(\Theta_1-\Theta_3) & a_4L_1\cos(\Theta_1-\Theta_4) & a_5L_1\cos(\Theta_1-\Theta_5) & a_6L_1\cos(\Theta_1-\Theta_6) & 0 & 0 & -a_1\sin(\Theta_1-\Phi) & a_1\cos(\Theta_1-\Phi) \\
a_2L_1\cos(\Theta_1-\Theta_2) & a_{11} & a_3L_2\cos(\Theta_2-\Theta_3) & a_4L_2\cos(\Theta_2-\Theta_5) & a_5L_2\cos(\Theta_2-\Theta_5) & a_6L_2\cos(\Theta_2-\Theta_6) & 0 & 0 & -a_2\sin(\Theta_2-\Phi) & a_2\cos(\Theta_2-\Phi) \\
a_3L_1\cos(\Theta_1-\Theta_3) & a_3L_2\cos(\Theta_2-\Theta_3) & a_{12} & a_4L_3\cos(\Theta_3-\Theta_4) & a_5L_4\cos(\Theta_3-\Theta_5) & a_6L_4\cos(\Theta_3-\Theta_6) & 0 & 0 & -a_3\sin(\Theta_3-\Phi) & a_3\cos(\Theta_3-\Phi) \\
a_4L_1\cos(\Theta_1-\Theta_4) & a_4L_2\cos(\Theta_2-\Theta_4) & a_4L_3\cos(\Theta_3-\Theta_4) & a_{13} & 0 & 0 & 0 & 0 & -a_4\sin(\Theta_4-\Phi) & a_4\cos(\Theta_4-\Phi) \\
a_5L_1\cos(\Theta_1-\Theta_5) & a_5L_2\cos(\Theta_2-\Theta_5) & a_5L_4\cos(\Theta_3-\Theta_5) & 0 & a_{14} & a_6L_5\cos(\Theta_5-\Theta_6) & 0 & 0 & -a_5\sin(\Theta_5-\Phi) & a_5\cos(\Theta_5-\Phi) \\
a_6L_1\cos(\Theta_1-\Theta_6) & a_6L_2\cos(\Theta_2-\Theta_6) & a_6L_4\cos(\Theta_3-\Theta_6) & 0 & a_6L_5\cos(\Theta_5-\Theta_6) & a_{15} & 0 & 0 & -a_6\sin(\Theta_6-\Phi) & a_6\cos(\Theta_6-\Phi) \\
0 & 0 & 0 & 0 & 0 & 0 & a_{16} & a_8L_7\cos(\Theta_7-\Theta_8) & -a_7\sin(\Theta_7-\Phi) & a_7\cos(\Theta_7-\Phi) \\
0 & 0 & 0 & 0 & 0 & 0 & a_8L_7\cos(\Theta_7-\Theta_8) & a_{17} & -a_8\sin(\Theta_8-\Phi) & a_8\cos(\Theta_8-\Phi) \\
-a_1\sin(\Theta_1-\Phi) & -a_2\sin(\Theta_2-\Phi) & -a_3\sin(\Theta_3-\Phi) & -a_4\sin(\Theta_4-\Phi) & -a_5\sin(\Theta_5-\Phi) & -a_6\sin(\Theta_6-\Phi) & -a_7\sin(\Theta_7-\Phi) & -a_8\sin(\Theta_8-\Phi) & a_9 & 0 \\
a_1\cos(\Theta_1-\Phi) & a_2\cos(\Theta_2-\Phi) & a_3\cos(\Theta_3-\Phi) & a_4\cos(\Theta_4-\Phi) & a_5\cos(\Theta_5-\Phi) & a_6\cos(\Theta_6-\Phi) & a_7\cos(\Theta_7-\Phi) & a_8\cos(\Theta_8-\Phi) & 0 & a_9
\end{bmatrix}
$$

Figure 27

BODY MATRIX

SECTION C.6

OUTPUT CALCULATIONS

The present output variables include the absolute accelerations of the centers of gravity of the head and chest, the conserved and dissipated energies in the separate parts, the kinetic energy, and the contact force position as well as all the positions, velocities, and accelerations of the vehicle and body segments. Under an output data option system, the output data desired could be chosen by the proper number in its option; which data are desired would be determined by the ultimate purpose for which the simulation is to be used.

The head and chest accelerations equations are, where i = 3 is the chest and i = 4 the head:

$$a_i(t) = \sqrt{\ddot{x}_i^2(t) + \ddot{y}_i^2(t)},$$

where

$$\ddot{x}_i(t) = x_h(t) - \sum_{m=1}^{i-1} L_m[\ddot{\alpha}_m(t)\sin\alpha_m(t)+\dot{\alpha}_m^2(t)\cos\alpha_m(t)]$$

$$- \rho_i[\ddot{\alpha}_i(t)\sin\alpha_i(t)+\dot{\alpha}_i^2(t)\cos\alpha_i(t)]$$

$$\ddot{y}_i(t) = y_h(t) + \sum_{m=1}^{i-1} L_m[\ddot{\alpha}_m(t)\cos\alpha_m(t)-\dot{\alpha}_m^2(t)\sin\alpha_m(t)]$$

$$+ \rho_i[\ddot{\alpha}_i(t)\cos\alpha_i(t)-\dot{\alpha}_i^2(t)\sin\alpha_i(t)].$$

The kinetic energy of the vehicle is:

$$KE_c(t) = \frac{1}{2}m_c[\dot{x}_c^2(t)+\dot{y}_c^2(t)] + \frac{1}{2}I_c\dot{\Phi}^2(t)$$

and of the individual body segments:

$$KE_i(t) = \frac{1}{2}m_i[u_i^2(t)+v_i^2(t)] + \frac{1}{2}I_i\dot{\alpha}_i^2(t)$$

for i = 1 to 8, where

$$i=1\text{-}4 \begin{cases} u_i(t) = \dot{x}_h(t) - \sum_{m=1}^{i-1} L_m\dot{\alpha}_m(t)\sin\alpha_m(t) - \rho_i\dot{\alpha}_i(t)\sin\alpha_i(t), \\ v_i(t) = \dot{y}_h(t) + \sum_{m=1}^{i-1} L_m\dot{\alpha}_m(t)\cos\alpha_m(t) + \rho_i\dot{\alpha}_i(t)\cos\alpha_i(t), \end{cases}$$

$$i=5,6 \begin{cases} u_i(t) = \dot{x}_h(t) - \sum_{m=1}^{2} L_m\dot{\alpha}_m(t)\sin\alpha_m(t) - L_4\dot{\alpha}_3(t)\sin\alpha_3(t) \\ \qquad - \sum_{m=5}^{i-1} L_m\dot{\alpha}_m(t)\sin\alpha_m(t) - \rho_i\dot{\alpha}_i(t)\sin\alpha_i(t), \\ v_i(t) = \dot{y}_h(t) + \sum_{m=1}^{2} L_m\dot{\alpha}_m(t)\cos\alpha_m(t) + L_4\dot{\alpha}_3(t)\cos\alpha_3(t) \\ \qquad + \sum_{m=5}^{i-1} L_m\dot{\alpha}_m(t)\cos\alpha_m(t) + \rho_i\dot{\alpha}_i(t)\cos\alpha_i(t), \end{cases}$$

$$i=7,8 \begin{cases} u_i(t) = \dot{x}_h(t) - \sum_{m=7}^{i-1} L_m\dot{\alpha}_m(t)\sin\alpha_m(t) - \rho_i\dot{\alpha}_i(t)\sin\alpha_i(t), \\ v_i(t) = \dot{y}_h(t) + \sum_{m=7}^{i-1} L_m\dot{\alpha}_m(t)\cos\alpha_m(t) + \rho_i\dot{\alpha}_i(t)\cos\alpha_i(t). \end{cases}$$

The conserved and dissipated energies in the seat are due to its springs, linear and nonlinear, and to the damper and friction; i.e.:

$$CE(t) = \frac{1}{2}\, s[y_1(t) + y_z(t) - z_o \tan\gamma_o]^2 + \frac{1}{2}\sum_{m=1}^{3} \frac{\beta_m y_1^{m+1}(t)}{m+1},$$

$$DE(t) = DE(t-\Delta t) + \frac{1}{2}\{c_s[\dot{y}_1(t)+\dot{y}_1(t-\Delta t)][y_1(t)-y_1(t-\Delta t)]$$

$$+ [f(t)+f(t-\Delta t)]\,[x_1(t)-x_1(t-\Delta t)]\}.$$

In the joints, the conserved energy is due to the elasticity and the dissipated to friction and restraints; thus for each joint (i = 1 to 7):

$$CE_i(t) = K_i[\theta_m(t)-\theta_i(t)+\theta_{io}-\theta_{mo}]^2,$$

$$DE_i(t) = \begin{cases} C_i'\left|\theta_m(t)-\theta_i(t) + \theta_{io} - \theta_{mo}\right| + \frac{1}{2}\sum_{t=0}^{t} [T_i(t) \\ \quad +T_i(t-\Delta t)][\theta_m(t)-\theta_m(t-\Delta t)-\theta_i(t)+\theta_i(t-\Delta t)] \\ \quad \text{for } \left|\dot{\theta}_m(t) - \dot{\theta}_i(t)\right| \geq \xi_i', \\ 0 \text{ otherwise.} \end{cases}$$

The gravitational energy is all conserved; for each body segment (i= 1 to 8):

$$CE_i(t) = gm_i[y_i^{cg}(t)\cos\Phi(t_m) - y_{io}^{cg}\cos\Phi(t)].$$

where

$$y_i^{cg}(t) = y_i(t) + \rho_i \sin\theta_i(t) \text{ for } i = 1 \text{ to } 6,$$

$$y_7^{cg}(t) = y_i(t) + \rho_7 \sin\theta_7(t),$$

$$y_8^{cg}(t) = y_7(t) + \rho_8 \sin\theta_8(t).$$

The conserved energy for each contact (i = 1 to 10) is $CE_i(t) = R_\ell E_i(t)$ (for proper ℓ); the dissipated energy is

$$DE_i(t) = (1-R_\ell)E_i(t).$$

The belt conserved energy is (for j = 1 to 3):

$$CE_j(t) = E_{cj}(t),$$

dissipated is:

$$DE_j(t) = \frac{(1-R_j)}{R_j} E_{cj}(t).$$

The last piece of output data at present is the contact force position, defined by $T_i(t)$ for i = 1 to 8.

SECTION C.7

END-OF-PROGRAM-TEST

The end-of-program option allows the selection of several tests. At present these choices are time only, time plus undesired contact, and time plus injury. Thus the time duration of the program run is always one of the criteria for the end-of-program test, and in fact is the only one contained in this section. It is shown in figure 28.

The undesired contact test is contained in Section C.4.f as Table 9 and in figure 20.

The injury test occurs in several places; that for joint dislocation due to excessive relative angle in Section C.4.c in figure 10 and the others in Section C.4.f, figure 20 and figure 26.

Another criterion that could be used as an end-of-program test is the cessation of body motion.

Which end-of-program test is chosen would depend in large part on what the simulation is being used for. If the purpose is to investigate or test various restraint systems, then time plus undesired contact would probably be the best criterion to use. If the interior vehicle design is the object, then the time plus injury criteria would be of value. If the purpose is just to find the motion, then time alone will be sufficient.

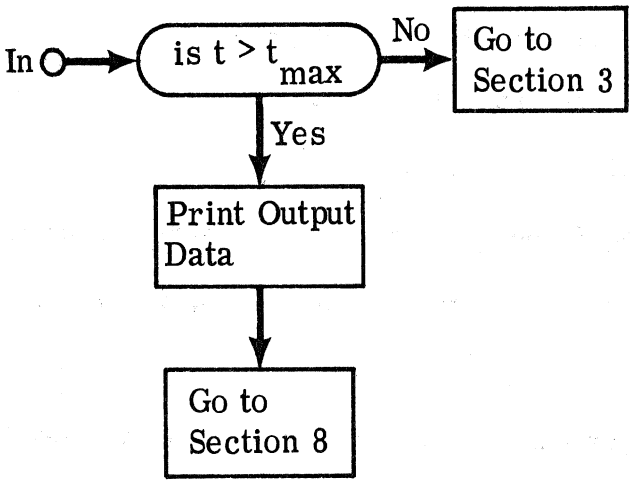

Figure 28

TIME END-OF-PROGRAM TEST

SECTION 8

MODIFICATIONS

It would be extremely useful for the program itself to be able to evaluate its own results, change certain input parameters or data, and then initiate a new run. The criteria for such evaluations and changes would depend on the ultimate use of the program, as would the selection of parameters to be varied.

For example, if the program were being used to evaluate restraint systems, then the natural parameters to be varied would be those of the belt material and their anchorage locations. The evaluation criteria could be the use of the undesired contact end-of-program test, the injury criteria for the torso and neck, and/or large forces in the belts themselves.

The method of changing the parameters could be either systematic or random, and they could be changed either singly or all at the same time.

SECTION D

A SIMPLE ANALOG TO COLLISION BETWEEN AUTO OCCUPANTS

The following describes a simple mathematical analog to the collision between front and rear auto occupants. The front seat occupant is restrained by a seat belt and shoulder harness whereas the rear seat occupant is restrained only by a seat belt. The simple model is shown in the following sketch.

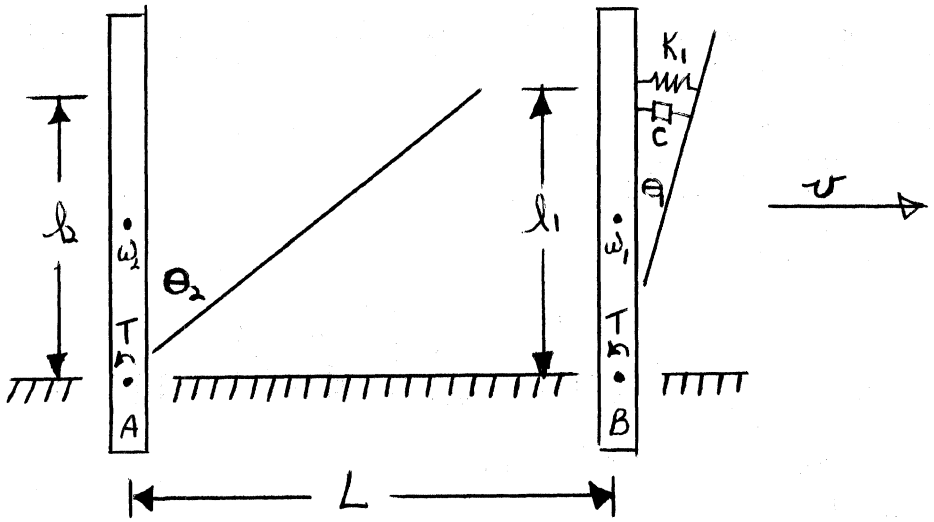

Points A and B represent the hip joints about which the upper portion of the bodies, w_1 and w_2 pivot due to the seat belt restraint. The rear seat occupant is restrained from pivoting only by the front seat back. For simplification, this is represented by a rigid stop when $\theta_2 \tilde{=} 60°$. The front seat occupant is restrained by a shoulder harness with spring and damping constants, k_1 and c. The angle θ_1 can reach a maximum of $\theta_1 = 14°$. The forward occupant is also restrained by a hip joint torque, T. It has been found that the inclusion of this

restraint on the rear occupant increases the amount of time between initial impact and final stop by about 8%. The initial forward velocity is v. The objective of the following is to show a simple analog to the difference between interoccupant motion in the cases where the front shoulder harness is an undamped spring and where it is critically damped.

The equation of motion for the front seat occupant is

$$I_0 \ddot{\theta}_1 + \ell_1 c\dot{\theta}_1 + \ell_1 k_1 \theta_1 \pm T = 0$$

The plus sign on T applies when $\dot{\theta}_1$ is positive. The undamped solution for initial conditions

$$\theta_1(0) = 0, \ \dot{\theta}_1(0) = \omega$$

is given by

$$\theta = \pm \frac{T}{\ell_1 k_1} \cos\left[\left(\frac{\ell_1 k_1}{I_0}\right)^{\frac{1}{2}} t\right] + \omega\left(\frac{I_0}{\ell_1 k_1}\right)^{\frac{1}{2}} \sin\left[\left(\frac{\ell_1 k_1}{I_0}\right)^{\frac{1}{2}} t\right] \mp \frac{T}{\ell_1 k_1}$$

For the critically damped case,

$$\theta = \pm \frac{T}{\ell_1 k_1} \exp\left(-\frac{\ell_1 c}{2I_0} t\right) + \left(\omega \pm \frac{Tc}{2k_1 I_0}\right) t \exp\left(-\frac{\ell_1 c}{2I_0} t\right) \mp \frac{T}{\ell_1 k_1}$$

The equations of motion and solution for the rear seat occupant under the same initial conditions are

$$I_0 \ddot{\theta}_2 = 0$$

$$\theta = \omega t$$

To make the situation as realistic as possible the system parameters have been determined as follows. The two occupants are assumed to be large (95th percentile males) with a weight of the upper part of the body of about 110 lb and a length of about 38 inces. The distance from

the pivot point to the center of gravity was taken to be 17 inches yielding $I_0 = 117$ lb-in-sec^2.

The initial angular velocity was found by noting that initially each body possessed a given linear momentum which had a moment of momentum about the pivot point of

$$mv\rho = I_0\omega$$

For a 20-mph collision, $\omega = 14.7$ rad/sec.

By trial and error it was found that a spring constant K = 25,000 lb/in. stopped motion of the forward occupant in 0.026 sec for the undamped case at about $\theta_1 \tilde{=} 14°$. Using the previously determined parameters the damping coefficient was found to be $c \tilde{=} 830$ lb-sec.

The motion in the undamped case proceded as follows. At t = 0.026 sec, the forward thrust of the front occupant had been arrested by the shoulder harness at $\theta_1 \tilde{=} 14°$. The rear occupant had pivoted to $\theta_2 \tilde{=} 22°$ in this time. The complete time history is:

time(sec)	θ_1(approx)	θ_2(approx)
0	0	0
0.026	14°	22°
0.050	1°	42°
0.068	- 8°	60°
0.075	-13°	60°

The simple sketch below shows that contact must have occurred between the two occupants between t = 0.050 and t = 0.075 if a typical seat separation (L = 34 inches) is used.

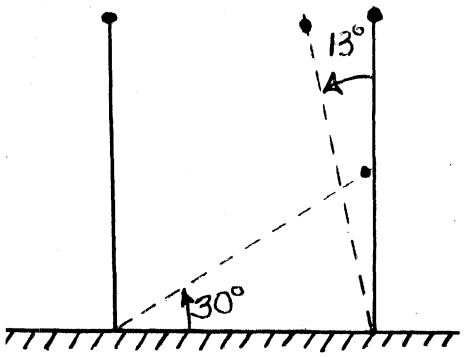

Dotted lines represent the final positions.

For the damped case numerical calculations show that the solution is dominated by the term

$$\Theta = \omega t \exp -\frac{\ell_1 ct}{2I_0}$$

This term is never negative, and thus the springback causing interoccupant collision using this model is impossible. By the time t = 0.125, $\Theta_1 \tilde{=} 1°$

The major objective of the simple study has been accomplished. The model has shown that collision between the two masses may or may not occur depending on system damping. Other parameters in the model besides damping will also play a major role. These are size of masses, pivot point location, rate of speed, geometry of restraints, pivot point restraint friction, etc., all of which are in the model and can be varied. These parameters can be considered analogous to size of occupant (not all drivers and occupants are 95th percentile male dummies), seat location, rate of speed, harness and seat belt geometry, joint friction, and seat design and properties.

REFERENCES

1. McHenry, R.R.: Analysis of the Dynamics of Automotive Passenger Restraint Systems. CAL No. VJ-1823-R1, May 31, 1963.

2. Naab, K.N.: A Computer Simulation of the Crash Victim-Comparison of the Results Obtained with Different Integration Routines, Time Increment Sizes, and Joint Friction Lags. CAL No. VJ-1823-R18, March 1966.

3. McHenry, R.R. and K.N. Naab: Computer Simulation of the Automobile Crash Victim in a Frontal Collision -- A Validation Study. CAL No. YB-2126-V-1, July 1966.

4. Smith, J.W.: Observations on the Postural Mechanism of the Human Knee Joint. Journal of Anatomy V.90 pt.2, p.236-261.

Acknowledgments are due to: Mark Berg for the list of parameters and basic variables and for the rigid-beam seat representation details, Prof. Kurt Binder for Figure 2, Dr. Verne Roberts for ideas and suggestions, Robert Bennett, Jr. for the computer programming, and Marcia Mascarello for calulations.